Electronic Supplementary Information

A Site-isolated Lewis Acidic Aluminum and Brønsted Basic Amine Sites in Dimeric Silsesquioxane Cage as a Reusable Homogeneous Bifunctional Catalyst for One-pot Tandem deacetalization/deketalization-Knoevenagel condensation Reactions

Pushparaj Loganathan,[a] Renjith S. Pillai,[a,b] Abigail Jennifer G,[a] Elumalai Varathan,[a] M. Kesavan,[c] Swaminathan Shanmugan*[a]

[a]Department of Chemistry, Faculty of Engineering and Technology, SRM Institute of Science and Technology, Kattankulathur-603203, Tamil Nadu, India.

E-mail: shanmugs2@srmist.edu.in, shanmugan0408@gmail.com

[b]Department of Chemistry, Christ University, Bangalore-56029, Karnataka, India.

[c]Interdisciplinary Institute of Indian System of Medicine (IIISM), SRM Institute of Science and Technology, Kattankulathur-603203, Tamil Nadu, India.

Contents

Fig. S8 (a) ^{29}Si NMR and (b) ^{27}Al NMR spectra of freshly prepared catalyst, reused catalyst after third and fifth cycles.

Table S7. Optimization of deketalization -Knoevenagel condensation reaction

^{1}H NMR spectra for compounds **6–6d**

^{13}C NMR spectra for compounds **6–6d**

LC-MS for compounds **6–6d**

^{1}H NMR of 2-(4-hydroxy-3-methoxybenzylidene)malononitrile

^{13}C NMR of 2-(4-hydroxy-3-methoxybenzylidene)malononitrile

LC-MS of 2-(4-hydroxy-3-methoxybenzylidene)malononitrile

Synthesis of 2-aryl-2-methyl-1,3-dioxolane (cyclic ketals) (**5–5d**)

Scheme S1. Synthesis of cyclic ketals (**5–5d**)

^{1}H NMR spectra for compounds **5–5d**

LC-MS for compounds **5–5d**

Synthesis of vanillin acetal

Scheme S2. Synthesis of vanillin acetal

^{1}H NMR spectrum of vanillin acetal

LC-MS of vanillin acetal

Table S1 Solubility of Al-POSS-NH_2 (**2**) in various organic solvents.

Solvents	Room Temperature	Heating condition
Methanol	Insoluble	Insoluble
Ethanol	Insoluble	Soluble
Acetonitrile	Insoluble	Insoluble
DMF	Insoluble	Soluble
Toluene	Soluble	Soluble
Benzene	Soluble	Soluble
Chloroform	Soluble	Soluble
DCM	Soluble	Soluble
THF	Soluble	Soluble
Hexane	Soluble	Soluble

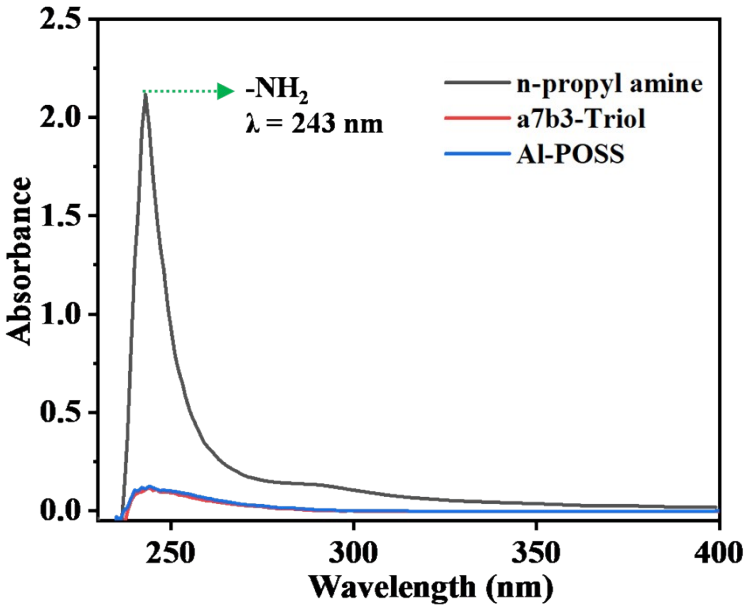

Fig. S1 UV-Vis spectra of *n*-propyl amine, Trisilanol heptaisobutyl-POSS and Al-POSS.

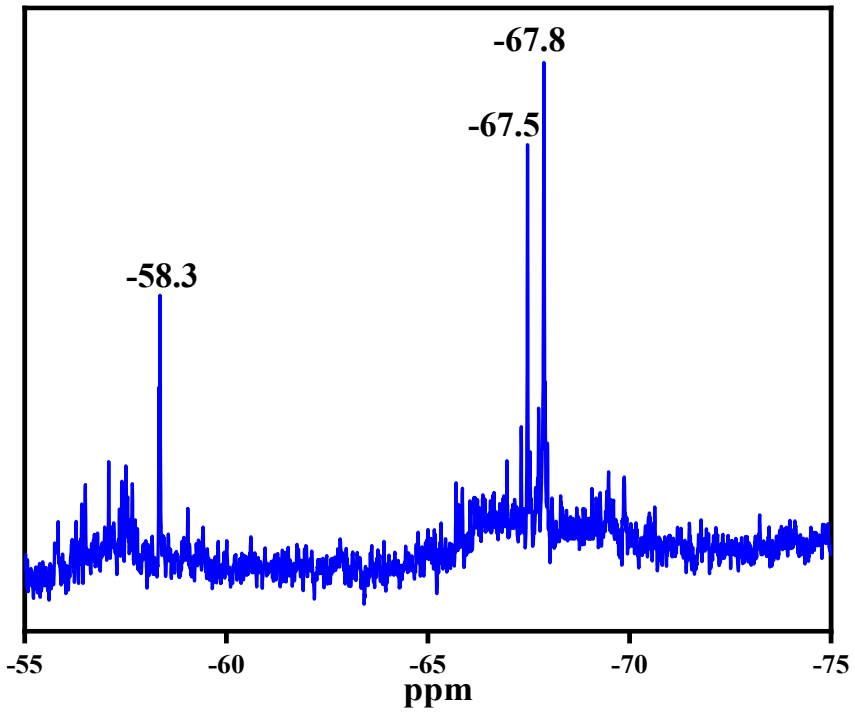

Fig. S2 ^{29}Si NMR spectrum of $(OH)_3$-a7b3-NH_2 (**1**)

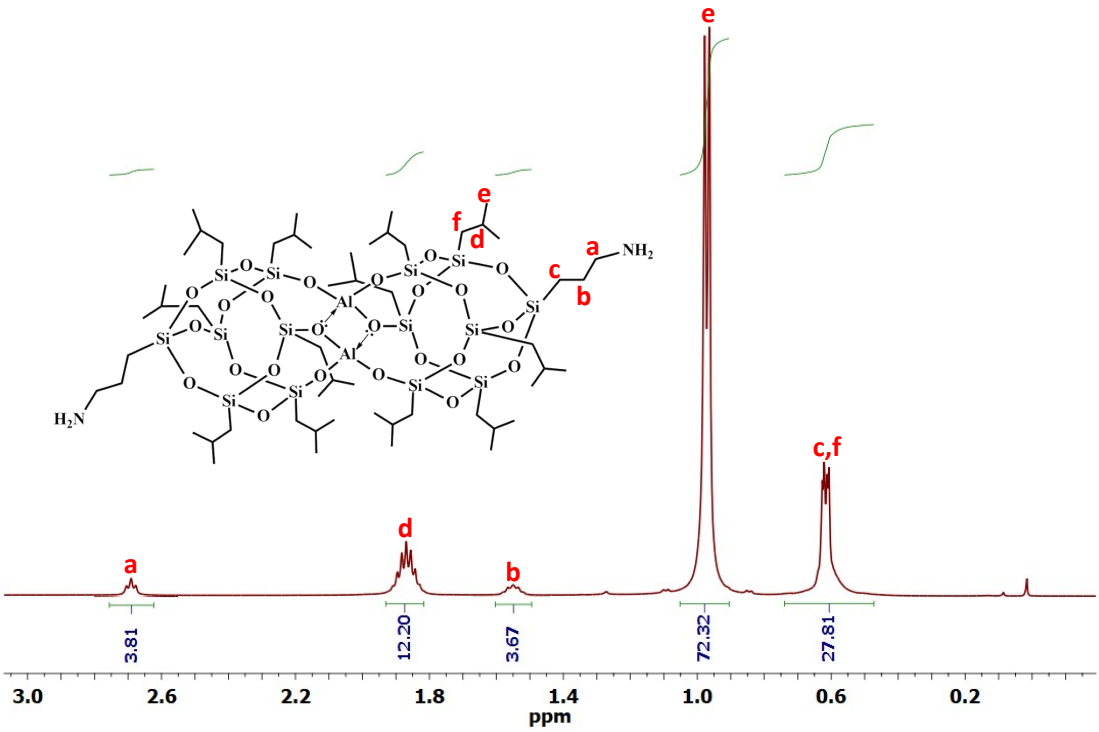

Fig. S3 ^{1}H NMR spectrum of Al-POSS-NH_2 (**2**)

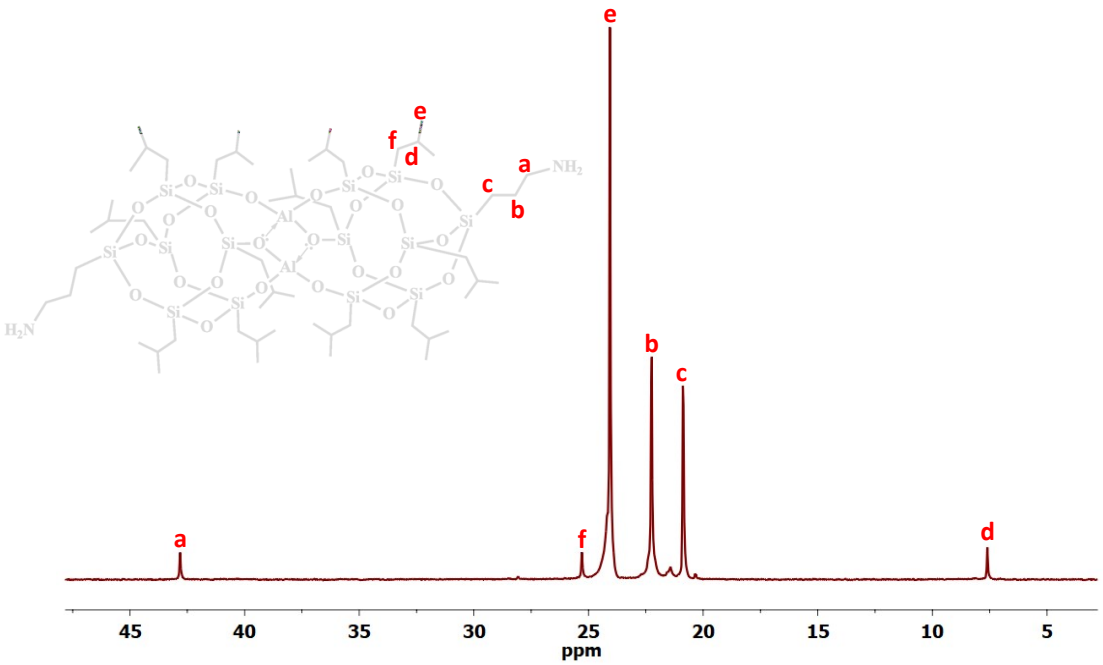

Fig. S4 ^{13}C NMR spectrum of Al-POSS-NH_2 (**2**).

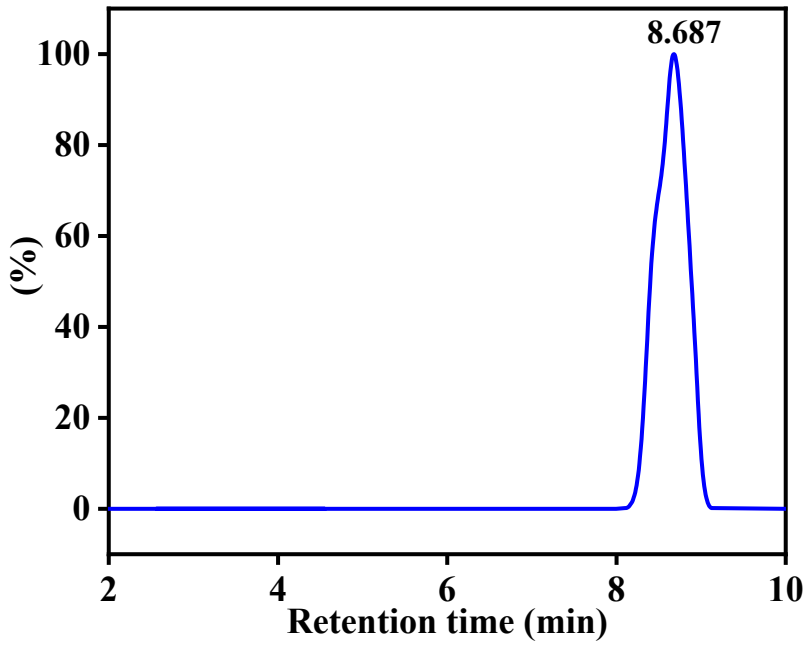

Fig. S5 GPC overlay graph of Al-POSS-NH_2 (**2**).

Table S2 Selected geometrical parameters of DFT optimized Al-POSS-NH_2 (**2**).

Table 2a BOND LENGTHS (in Å)			
Al-O bonds			
Al(1)-O(1)	**Al(1)-O(4)**	**Al(1)-O(4A)**	**Al(1A)-O(9)**
1.702	1.842	1.844	1.701
Si-O bonds			
Si(1)-O(1)	**Si(1)-O(2)**	**Si(1)-O(10)**	**Si(2)-O(2)**
1.618	1.652	1.642	1.630
Si(2)-O(3)	**Si(2)-O(12)**	**Si(3)-O(4)**	**Si(3)-O(3)**
1.663	1.637	1.688	1.631
Si(3)-O(10)	**Si(4)-O(11)**	**Si(5)-O(6)**	**Si(5)-O(7)**
1.638	1.620	1.634	1.647
Si(6)-O(8)	**Si(7)-O(5)**	**Si(7)-O(8)**	**Si(7)-O(9)**
1.639	1.648	1.658	1.619
C-N and N-H bonds			
C(1)-N(1)	**N(1)-H(1)**	**C(1)-N(1)**	**N(1)-H(1)**
1.47	1.02	1.47	1.02

Table 2b BOND ANGLES (in ^{O})			
∠Al(1)-O-Al(1A)	**∠Al(1)-O(1)-Si(1)**	**∠Al(1)-O(4)-Si(3)**	**∠Al(1A)-O(9)-Si(7)**
96.41	143.88	129.97	149.6
∠Al-(1A)-O(4)-Si(3)	**∠O(12)-Si(5)-O(7)**	**∠O(6)-Si(5)-O(7)**	**∠O(7)-Si(6)-O(8)**
133.63	107.87	110.29	109.17
∠Si(7)-O(8)-Si(6)	**∠Si(6)-O(11)-Si(4)**	**∠Si(6)-O(7)-Si(5)**	**∠Si-(5)-O(12)-Si(2)**
155.33	142.75	148.96	155.93
∠Si(5)-O(6)-Si(4)	**∠Si(4)-O(5)-Si(7)**	**∠Si(2)-O(2)-Si(1)**	**∠Si(2)-O(3)-Si(3)**
155.93	146.27	141.16	167.54
∠Si(3)-O(10)-Si(1)	**∠O(1)-Si(1)-O(2)**	**∠O(2)-Si(2)-(O12)**	**∠O(3)-Si(2)-O(12)**
149.84	110.01	108.95	108.90
∠O(7)-Si(6)-O(11)	**∠O(8)-Si(7)-O(9)**	**∠O(8)-Si(7)-O(5)**	**∠O(5)-Si(4)-O(10)**
109.55	109.29	109.28	108.12
∠O(10)-Si(1)-O(2)	**∠O(10)-Si-(1)-O(1)**	**∠O(10)-Si(3)-O(6)**	**∠O(6)-Si(4)-O(5)**
109.4	106.96	109.07	109.84
∠O(7)-Si(5)-O(12)	**∠O(6)-Si(5)-O(12)**	**∠O(6)-Si(3)-O(10)**	**∠O(4)-Si(3)-O(3)**
107.87	109.77	109.07	106.23
∠H(2)-N(1)-H(1)	**∠C(1)-N(1)-H(1)**		
106.18	108.9		

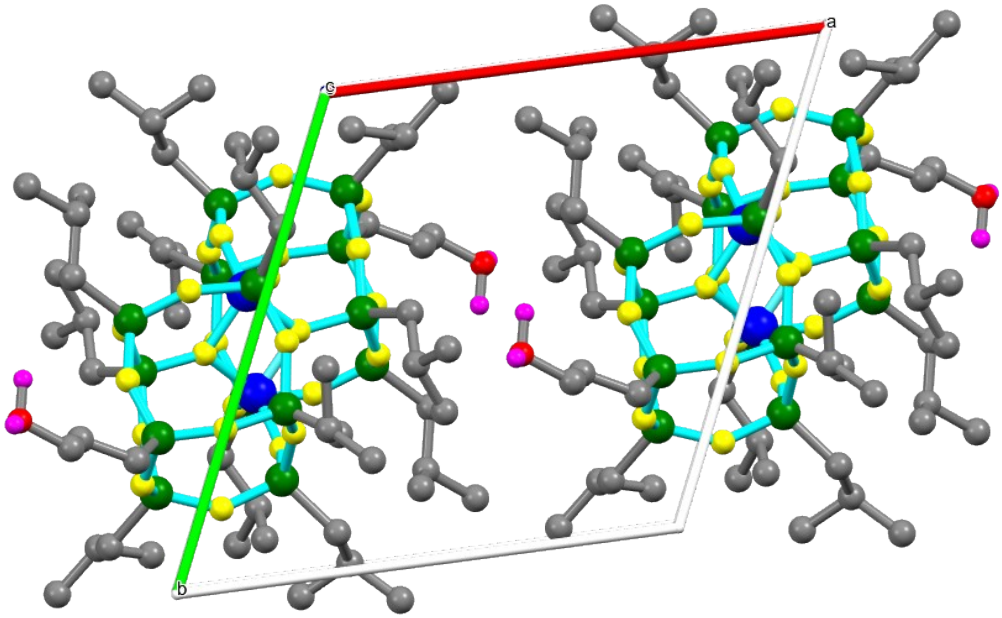

Fig. S6 DFT optimized unit cell structure of Al-POSS-NH_2 (**2**) viewed along *b* vector direction.

Table S3 Charges (e) on atoms of atoms of Al-POSS-NH_2 (**2**) computed at PBE-D/TZ2P level of theory using ADF

Atoms	VDD	Hirshfeld	Mulliken
Al(1)/Al(1A)	0.461	0.534	1.199
Si(1)/Si(1A)	0.411	0.482	1.536
Si(2)/Si(2A)	0.416	0.495	1.491
Si(3)/Si(3A)	0.419	0.511	1.469
Si(4)/Si(4A)	0.494	0.411	1.493
Si(5)/Si(5A)	0.426	0.499	1.465
Si(6)/Si(6A)	0.416	0.499	1.465
Si(7)/Si(7A)	0.411	0.485	1.529
C(1)/C(1A)	-0.030	-0.028	0.507
N(1)/N(1A)	-0.216	-0.225	-0.094
H(1/2)/H(1A/2A)	0.093	0.098	-0.049
O(1)/O(1A)	-0.373	-0.347	-0.823

O(2)/O(2A)	-0.293	-0.286	-0.760
O(3)/O(3A)	-0.251	-0.275	-0.756
O(4)/O(4A)	-0.247	-0.272	-0.947
O(5)/O(5A)	-0.293	-0.283	-0.756
O(6)/O(6A)	-0.266	-0.282	-0.754
O(7)/O(7A)	-0.274	-0.283	-0.754
O(8)/O(8A)	-0.271	-0.280	-0.763
O(9)/O(9A)	-0.371	-0.350	-0.814
O(10)/O(10A)	-0.277	-0.281	-0.774
O(11)/O(11A)	-0.269	-0.275	-0.768
O(12)/O(12A)	-0.292	-0.291	-0.751

Table S4 Electron density (ρ_c) (in e/bohr^3)) values computed at the bond critical points (BCPs) using QTAIM

ρ_c (e/bohr^3) at Al-O BCP			
Al(1)-O(1)	**Al(1)-O(4)**	**Al(1)-O(4A)**	**Al(1A)-O(9)**
0.110	0.077	0.077	0.110
ρ_c (e/bohr^3) at Si-O BCP			
Si(1)-O(1)	**Si(1)-O(2)**	**Si(1)-O(10)**	**Si(2)-O(2)**
0.152	0.136	0.138	0.143
Si(2)-O(3)	**Si(2)-O(12)**	**Si(3)-O(4)**	**Si(3)-O(3)**
0.137	0.142	0.129	0.147
Si(3)-O(10)	**Si(4)-O(11)**	**Si(5)-O(6)**	**Si(5)-O(7)**
0.146	0.143	0.143	0.140
Si(6)-O(8)	**Si(7)-O(5)**	**Si(7)-O(8)**	**Si(7)-O(9)**
0.145	0.141	0.136	0.152
ρ_c (e/bohr^3) at C-N and N-H BCP			
C(1)-N(1)	**N(1)-H(1)**	**C(1A)-N(1A)**	**N(1A)-H(1A)**
0.258	0.337	0.259	0.337

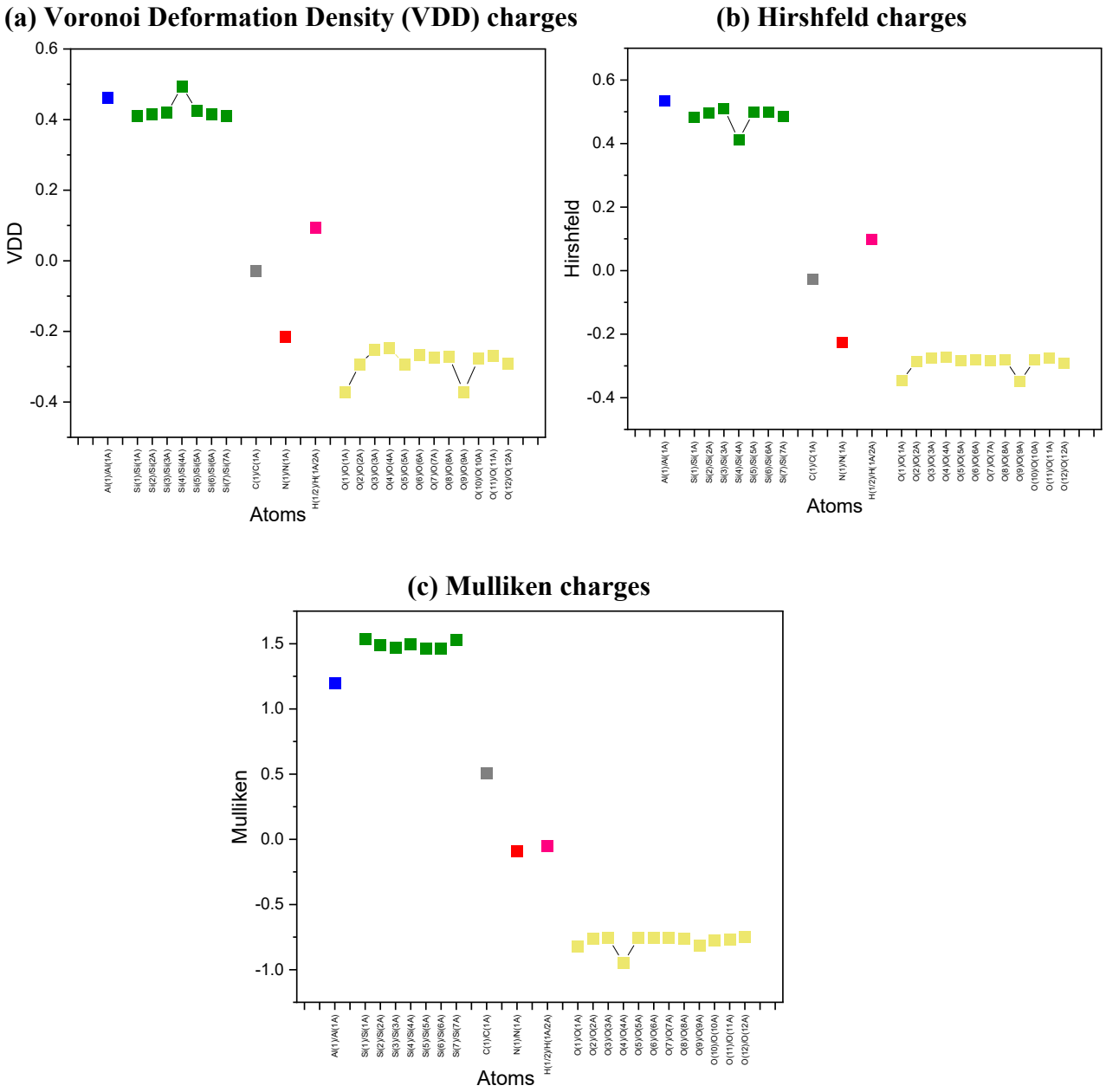

Fig. S7 The atomic charges (e) of Al-POSS-NH_2(**2**) in different methods at PBE-D/TZ2P level of theory using ADF 2019.305. (a) Voronoi Deformation Density (VDD) charges (b) Hirshfeld charges (c) Mulliken charges. Atom colours: Al - blue, Si - Green, O - yellow, N - Red, C – Gray, H – Violet

DFT Calculations

The starting geometry for Al-POSS-NH_2 (**2**) unit cell was modelled and optimized in the gas phase at the density functional theory (DFT) level using the CP2K code.[1] For

geometry optimization, the Perdew-Burke-Ernzerhof (PBE)[2] DFT functional with semi-empirical dispersion remedies, as used in the DFT-D3 approach[3] (i.e., Grimme's D3 dispersion corrections) was used to account for the van der Waals interactions.[4] Split Gaussian basis set was used, where a triple zeta (TZVP-MOLOPT) basis set was employed for carbon, oxygen, and hydrogen whereas a double zeta (DZVP-MOLOPT) basis set was applied to silicon and aluminum.[5] The pseudo potentials derived by Goedecker, Teter, and Hutter were used for all the atoms in Al-POSS-NH_2. On geometry optimization the atomic position of the framework was completely relaxed while the parameters of the unit cell were maintained at their empirically determined values. Further, coordinates of the optimized geometry were used to compute the electron density topology and charges based on the natural population using single-point energy calculations in DFT method employed in the Amsterdam Density Functional (ADF) software package, version 2019.305.[6] For these analyses, PBE functional with Grimme's dispersion corrections, i.e., PBE-D3 was used along with triple zeta double potential (TZ2P) basis set. The partitioning of electron density at zero flux surfaces (e.g., at the bond path between two atoms, called the bond critical point (BCP)) was given by Bader's quantum theory of atoms in molecules (QTAIM) analysis.[8,9] The charges on Al, Si, O, N, C and H (of the amines) were obtained from different methods,[10] such as Voronoi Deformation Density (VDD) charge, Hirshfeld charge, and Mulliken charge.

Table S5. Optimization of deacetalization-Knoevenagel condensation reaction

Entry	Solvents	Catalyst (mol%)	Time (hours)	Conv of A (%)	Isolated Yield %	TON
1	Acetonitrile	1	3	5	3	10
			6	9	6	20
			9	10	8	26
2	Acetonitrile	3	3	13	10	33
			6	15	12	40
			9	18	15	50
3	Acetonitrile	6	3	20	18	60
			6	25	20	66
			9	30	23	76
4	1,4-dioxane	1	3	10	5	16
			6	18	12	40
			9	23	18	60
5	1,4-dioxane	3	3	25	21	70
			6	31	28	93
			9	41	37	123
6	1,4-dioxane	6	3	30	27	90
			6	40	38	126
			9	46	40	133
7	Toluene	1	3	18	10	33
			6	31	25	83
			9	46	41	136
8	Toluene	3	3	35	30	100
			6	54	51	170
			9	65	60	200
9	Toluene	6	3	50	40	133
			6	70	66	220
			9	82	75	250
10	DMF	1	3	45	41	136
			6	56	49	160
			9	65	60	200
11	DMF	3	3	88	80	260
			6	100	99	330
			9	100	99	330

One-pot Tandem Deacetalization-Knoevenagel Condensation Reactions

Gas Chromatograms:

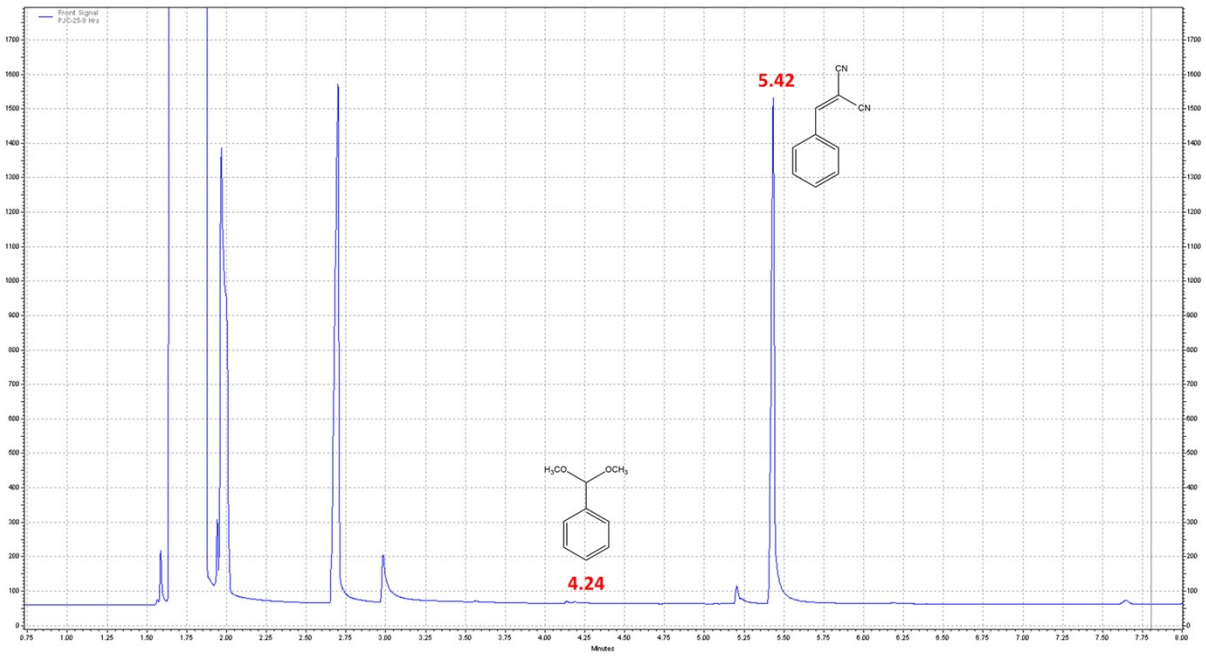

GC of compound **4**

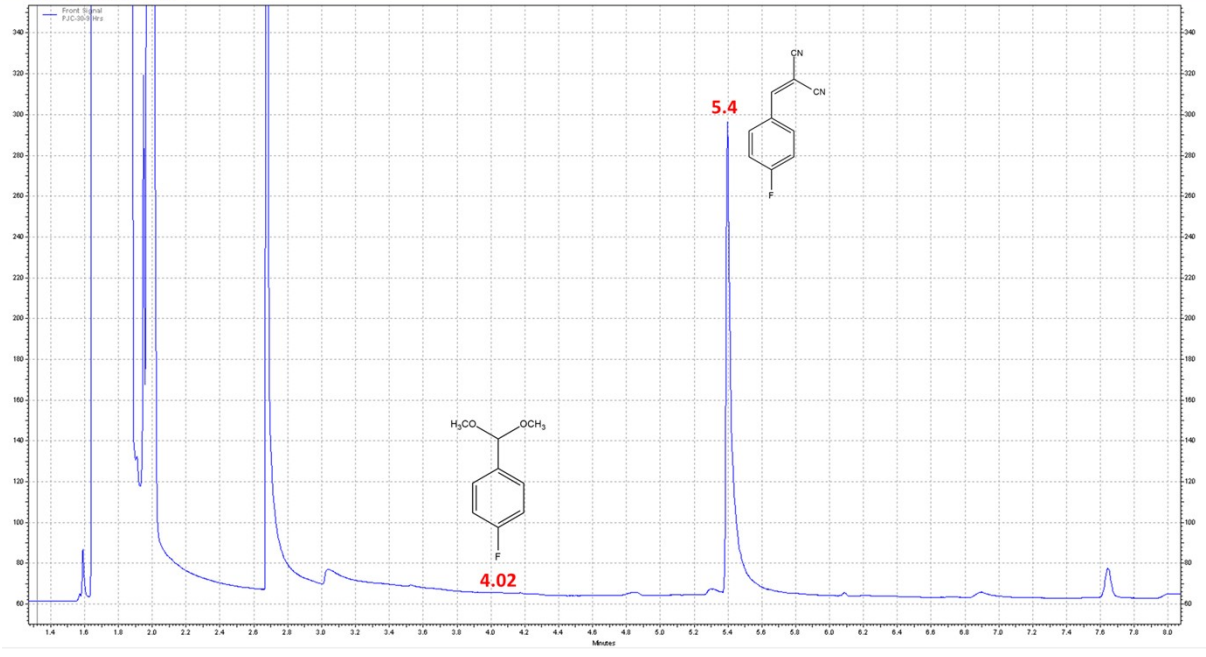

GC of compound **4a**

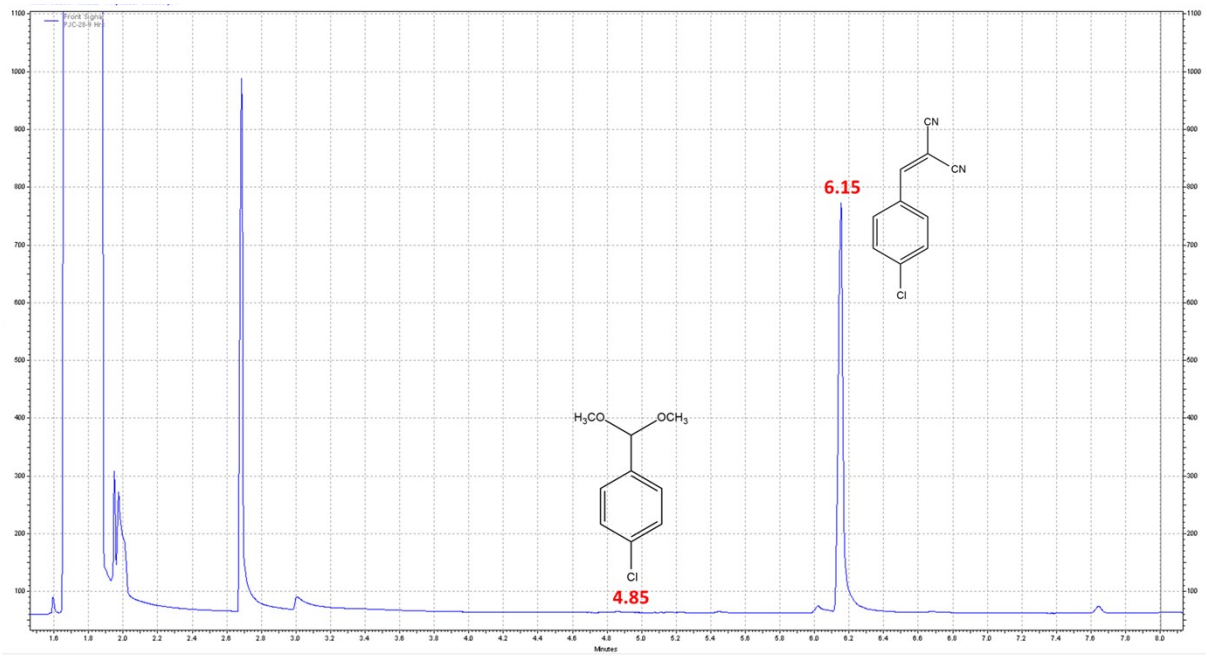

GC of compound **4b**

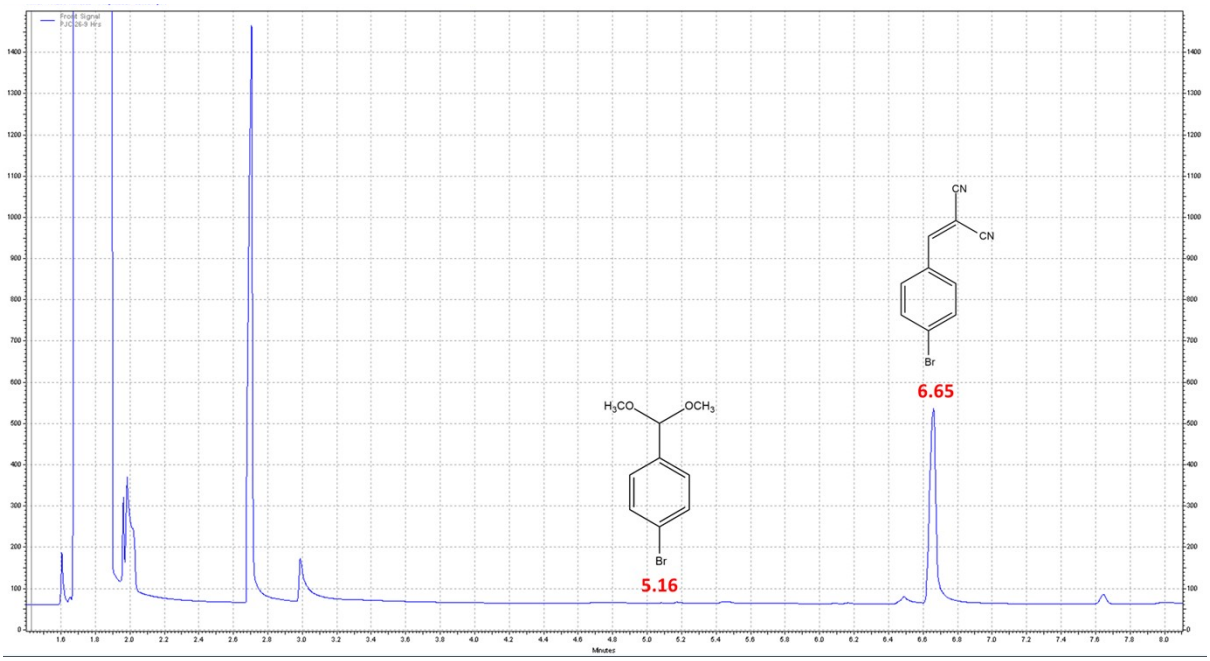

GC of compound **4c**

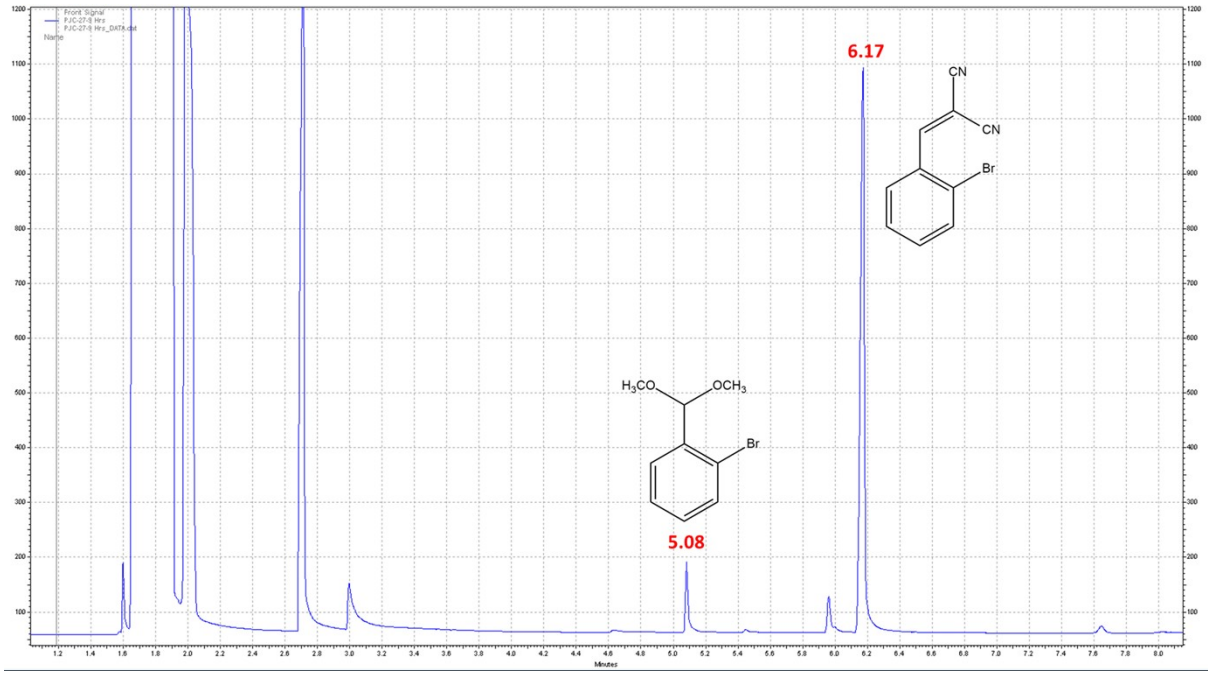

GC of compound **4d**

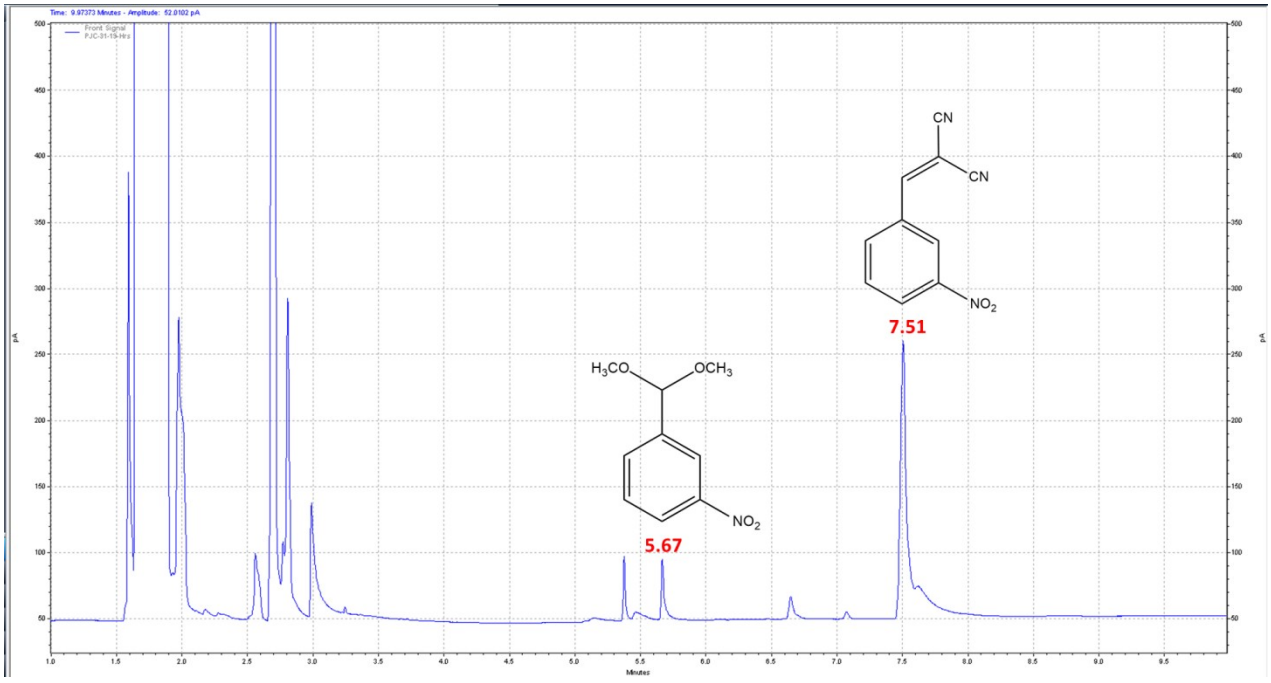

GC of compound **4e**

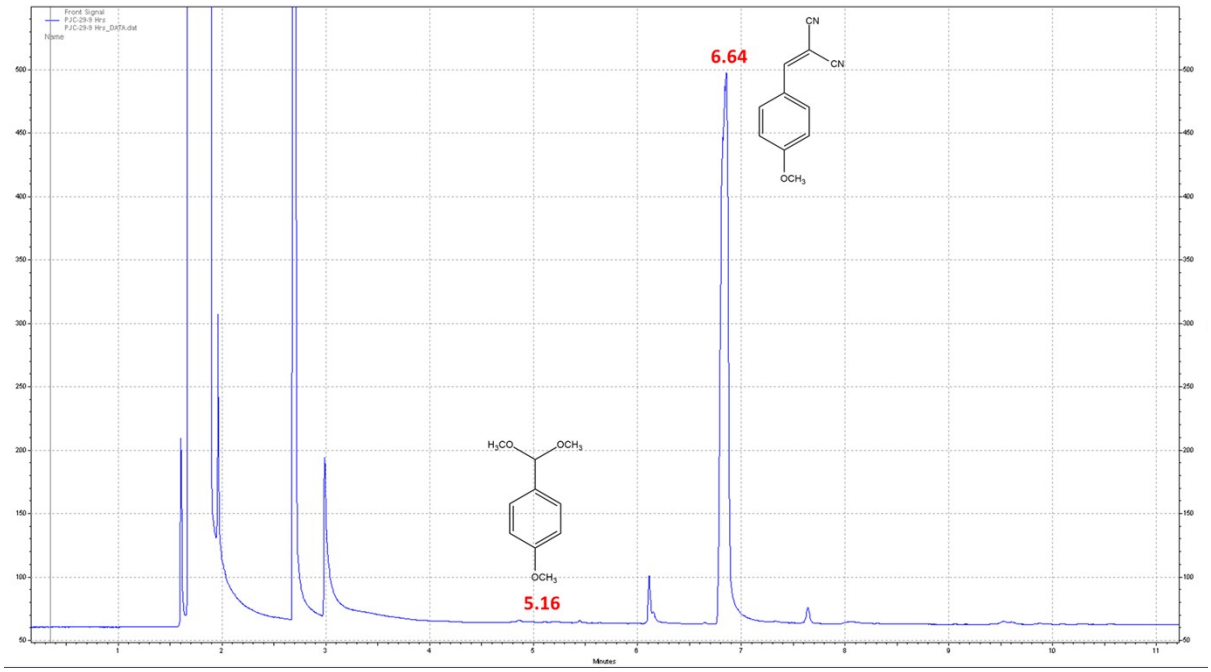

GC of compound **4f**

[1]H NMR Spectra:

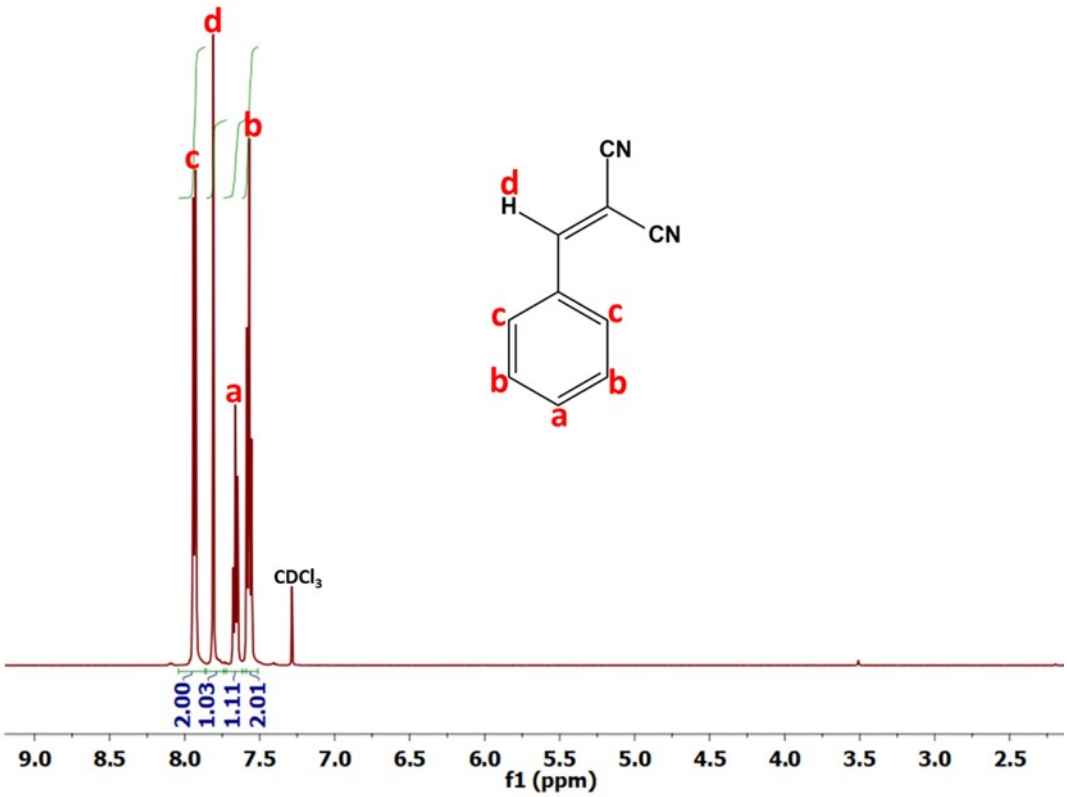

[1]H NMR spectrum of compound **4** in $CDCl_3$

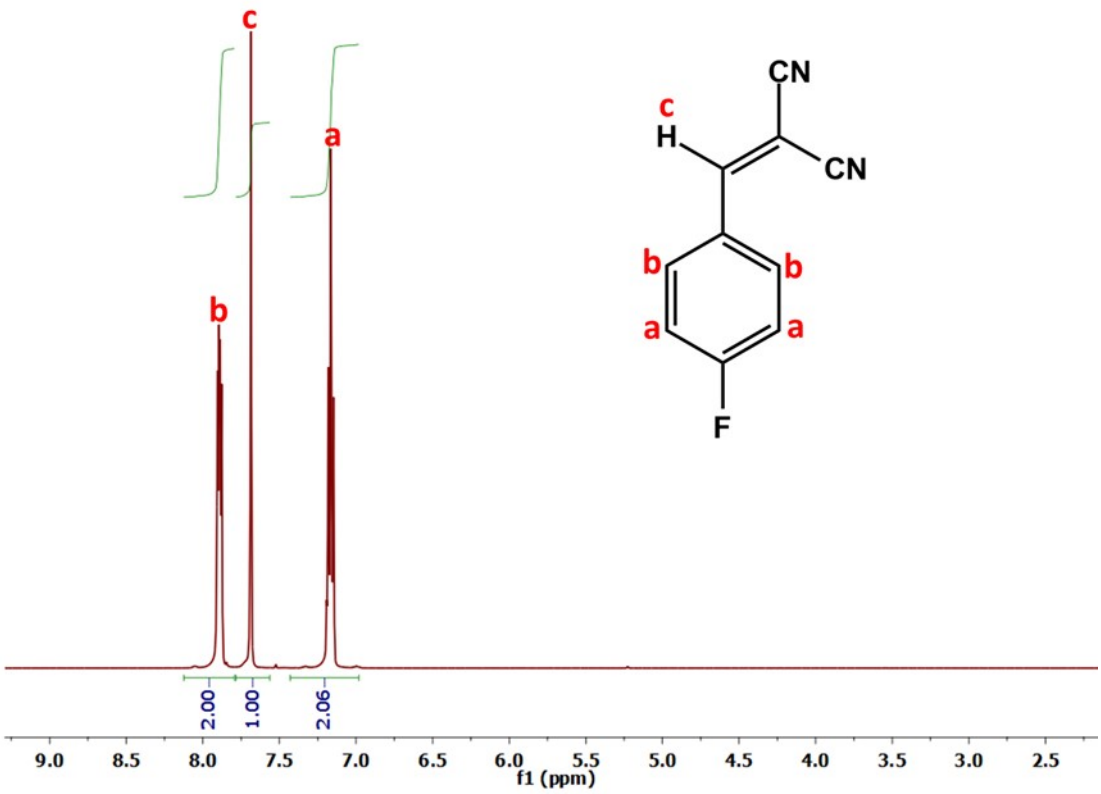

^{1}H NMR spectrum of compound **4a** in $CDCl_3$

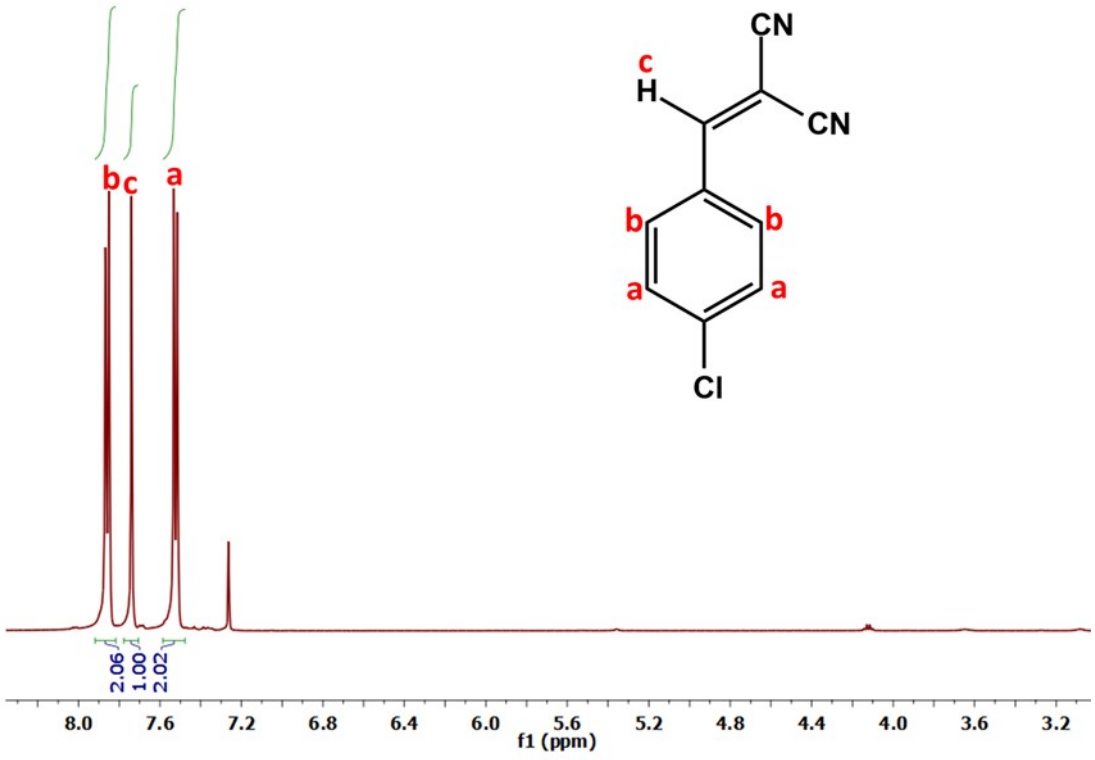

^{1}H NMR spectrum of compound **4b** in $CDCl_3$

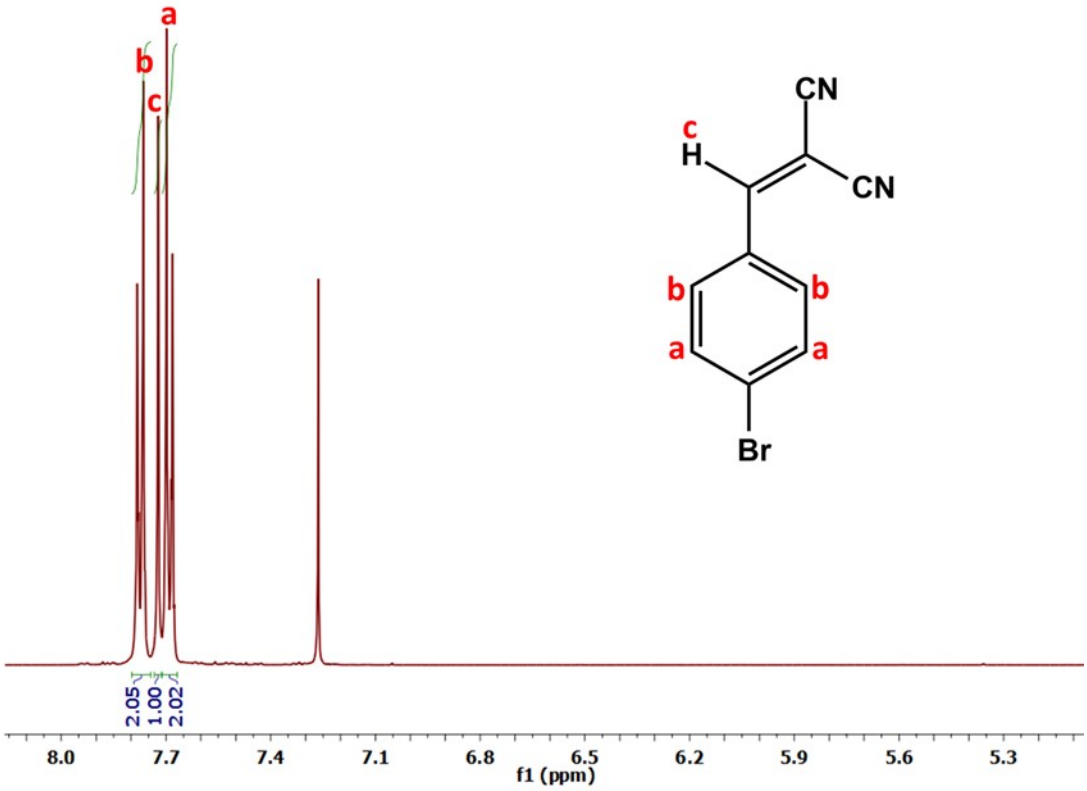

^{1}H NMR spectrum of compound **4c** in $CDCl_3$

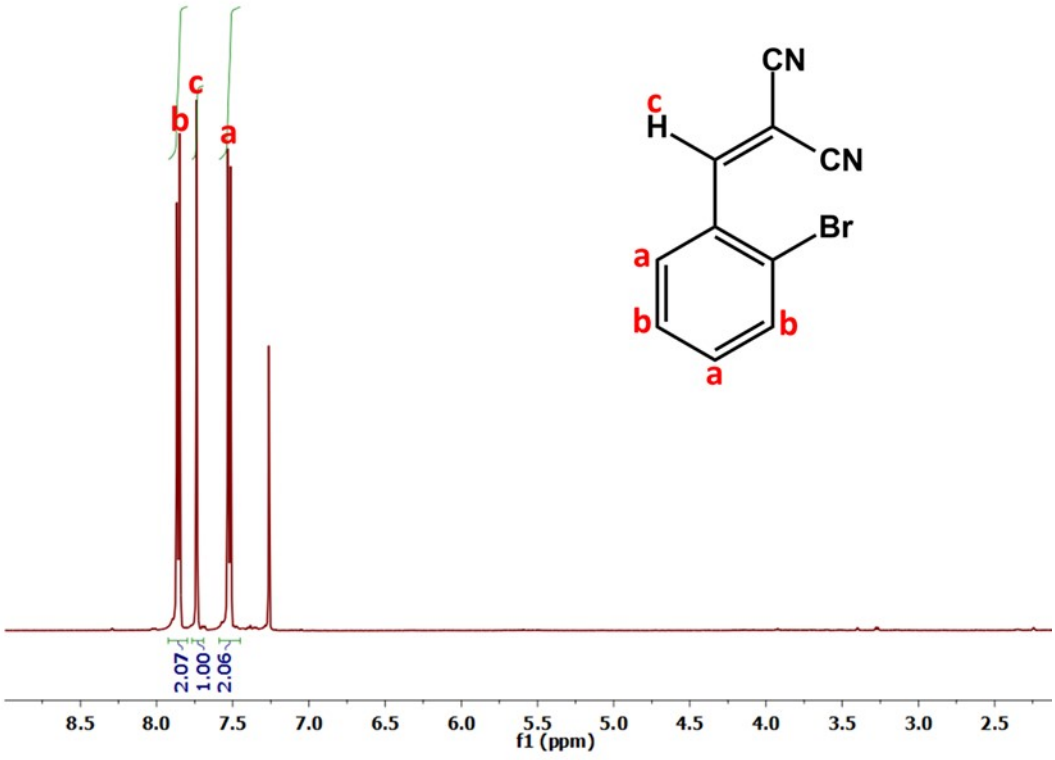

^{1}H NMR spectrum of compound **4d** in $CDCl_3$

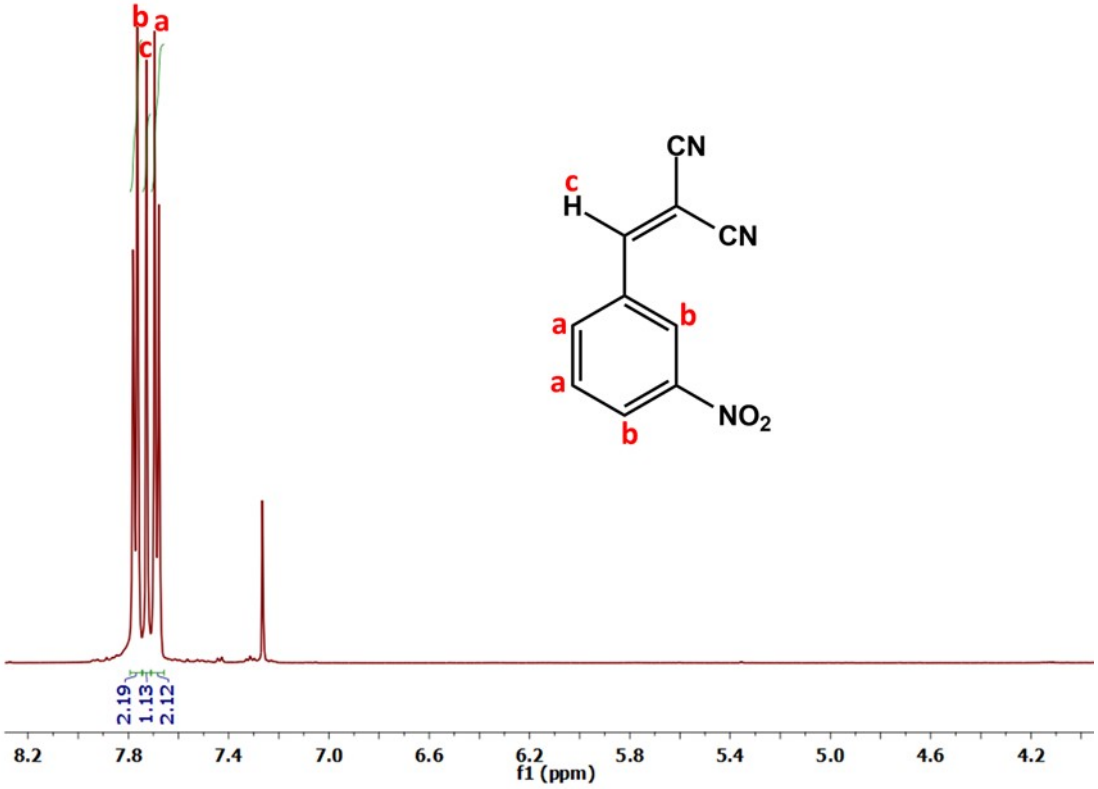

^{1}H NMR spectrum of compound **4e** in $CDCl_3$

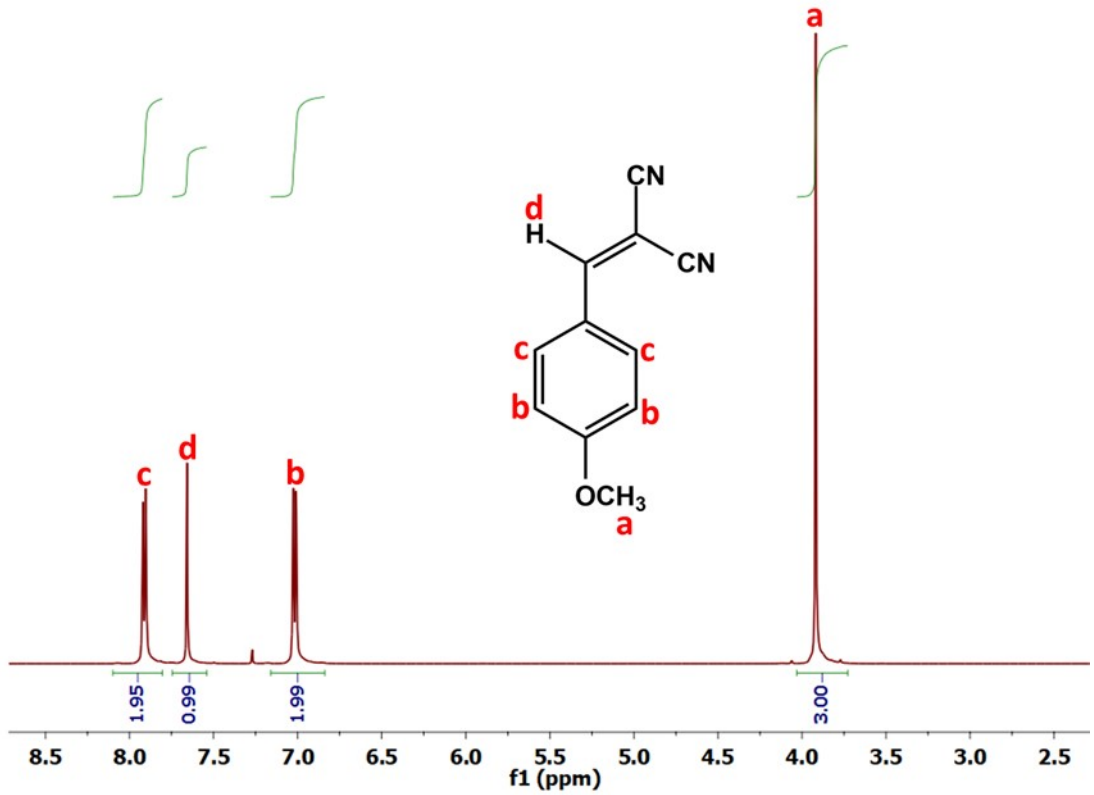

^{1}H NMR spectrum of compound **4f** in $CDCl_3$

^{13}C NMR Spectra:

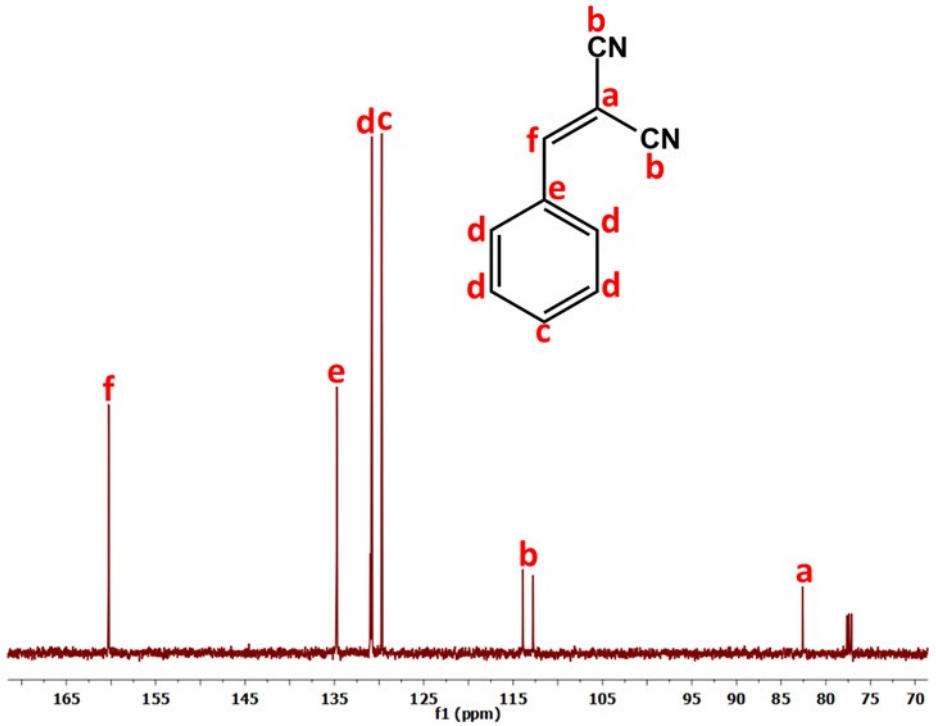

^{13}C NMR spectrum of compound **4** in $CDCl_3$

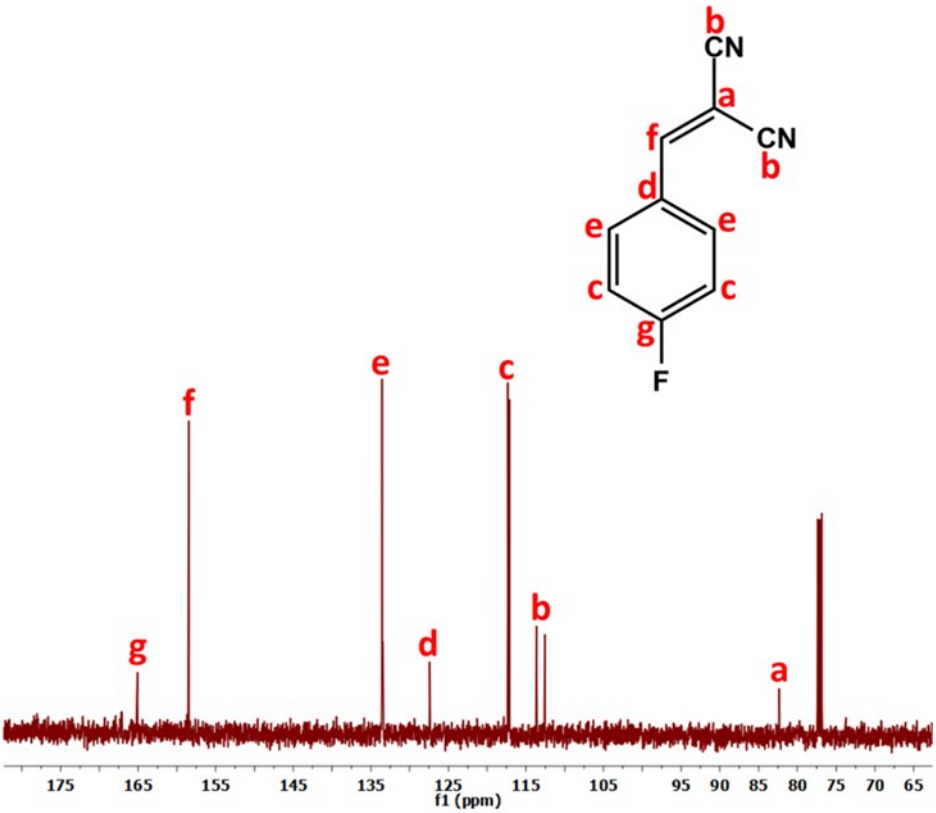

^{13}C NMR spectrum of compound **4a** in $CDCl_3$

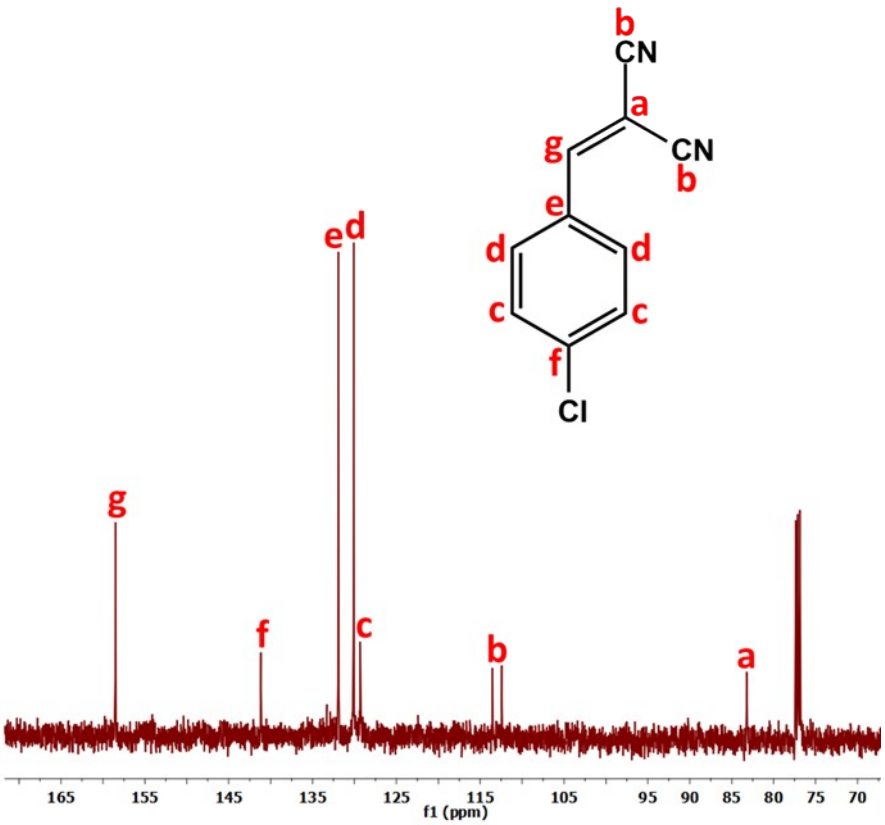

^{13}C NMR spectrum of compound **4b** in $CDCl_3$

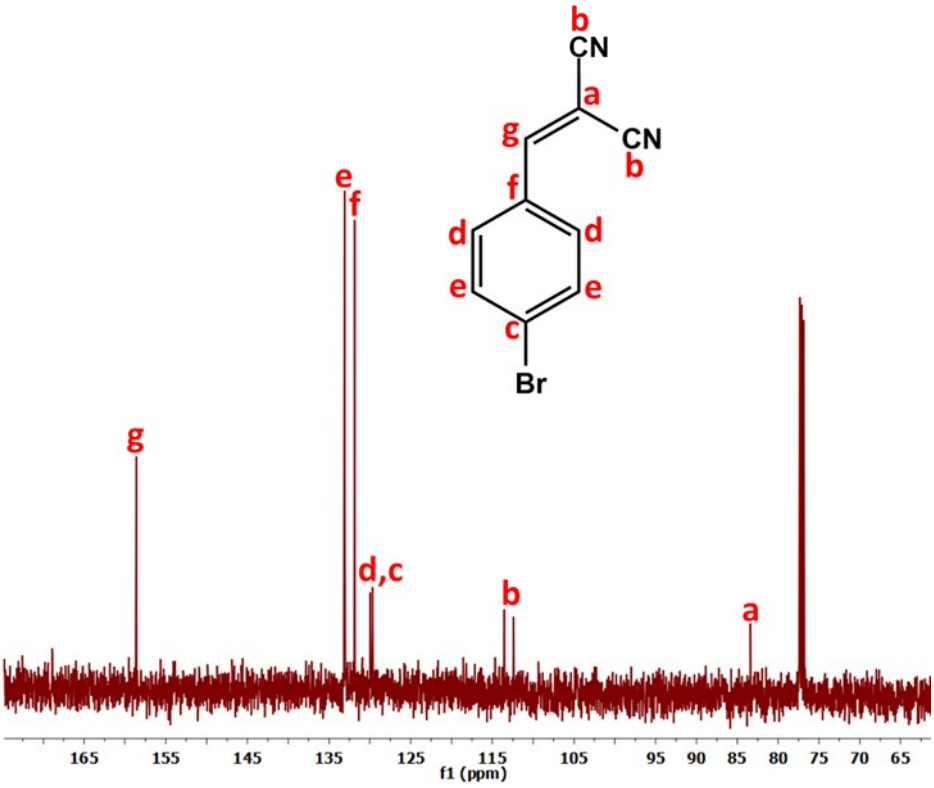

^{13}C NMR spectrum of compound **4c** in $CDCl_3$

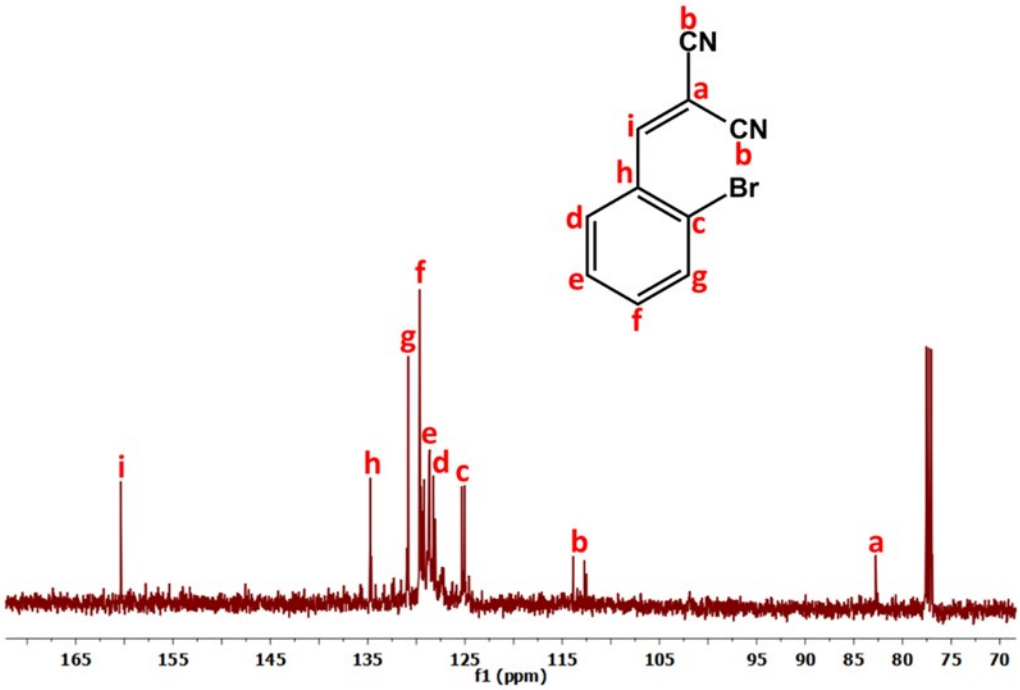

^{13}C NMR spectrum of compound **4d** in $CDCl_3$

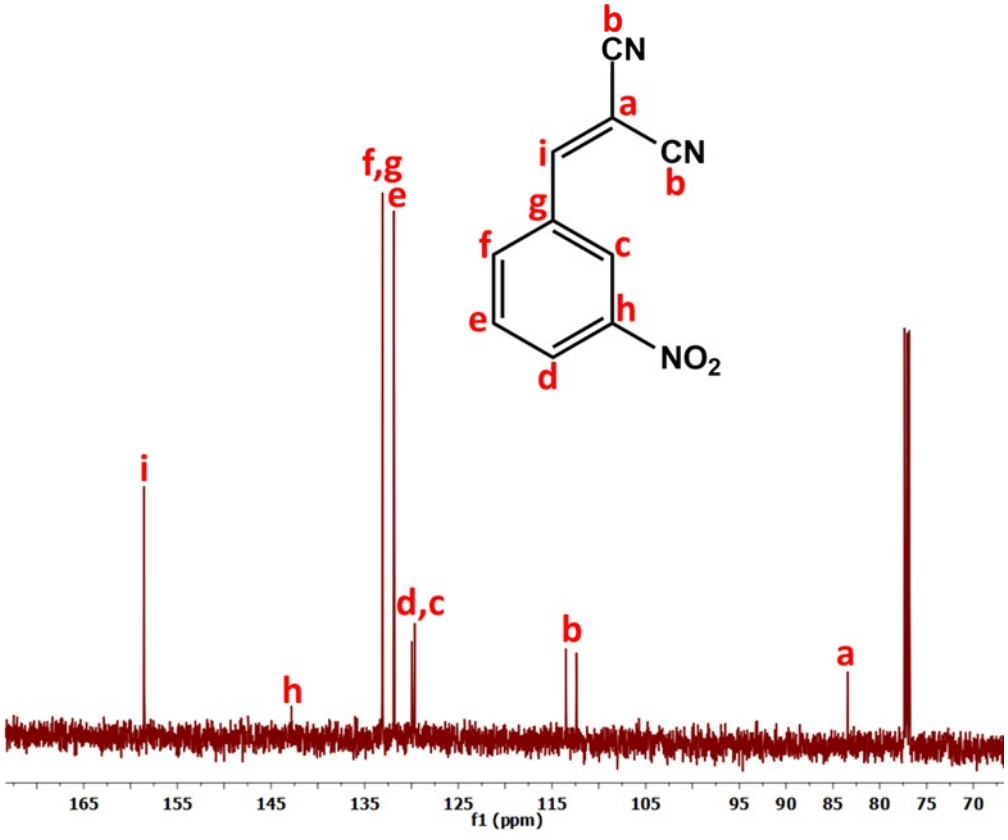

^{13}C NMR spectrum of compound **4e** in $CDCl_3$

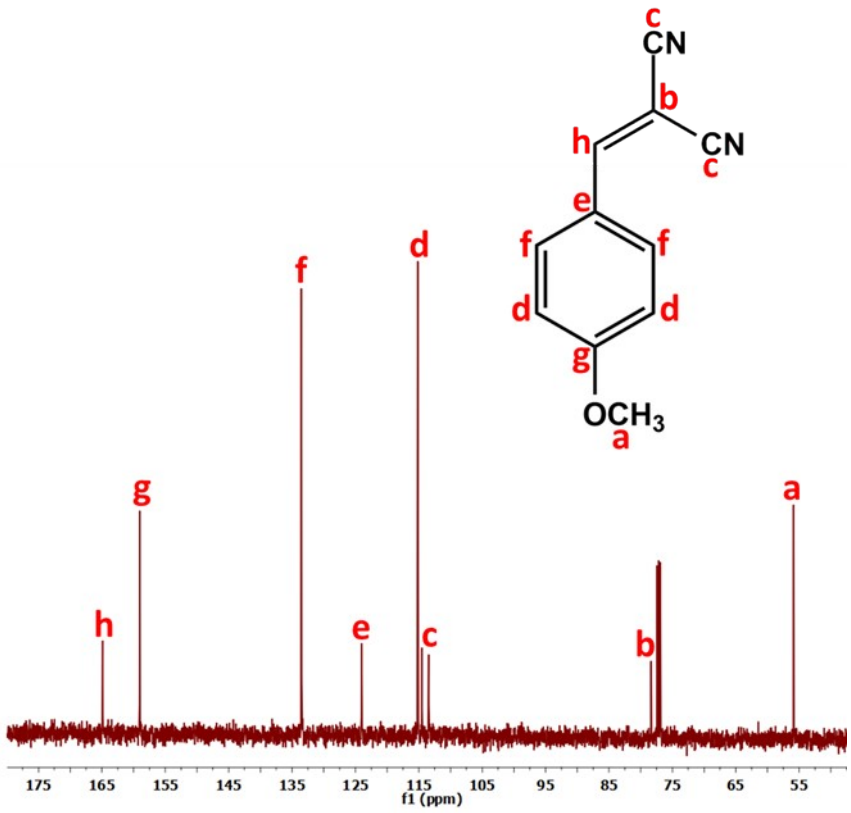

^{13}C NMR spectrum of compound **4f** in $CDCl_3$

LC-MS:

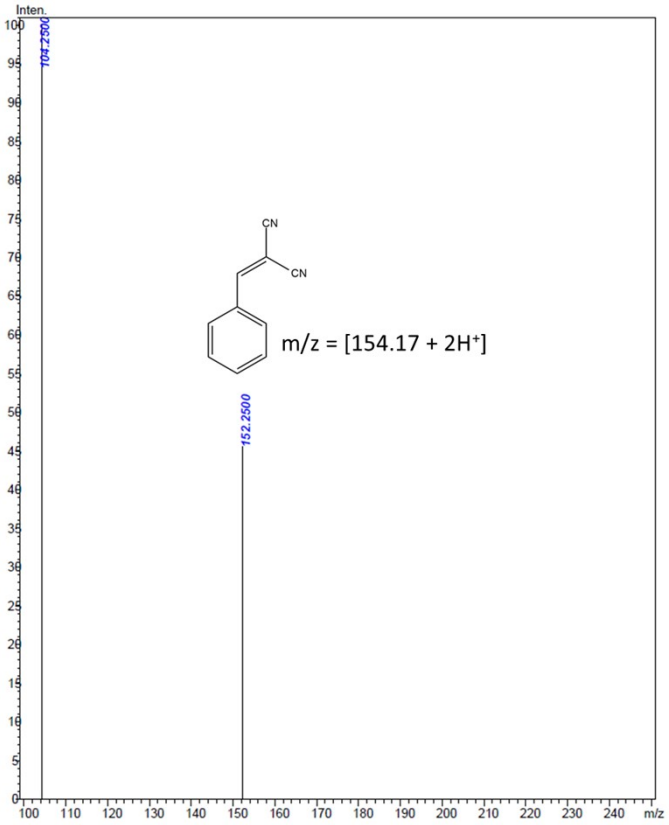

LC-MS of compound **4**

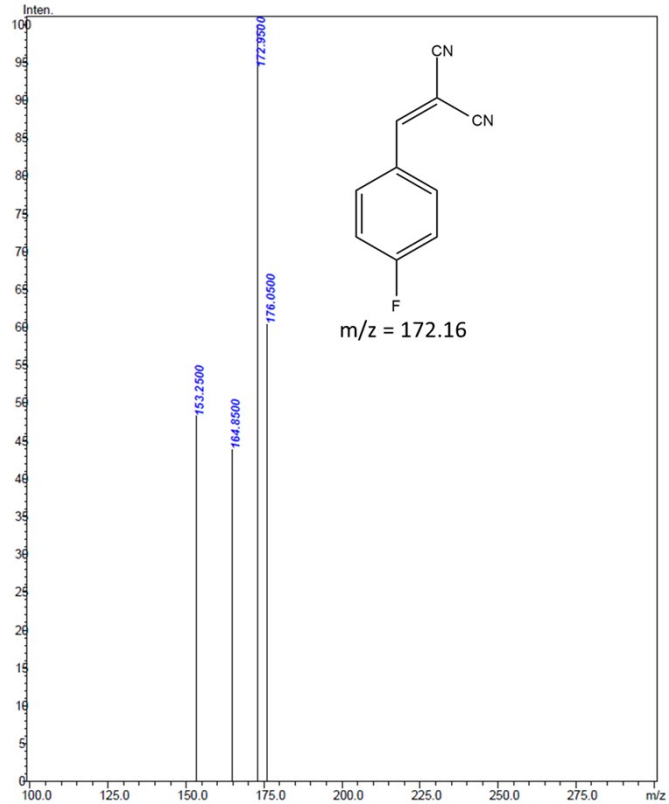

LC-MS of compound **4a**

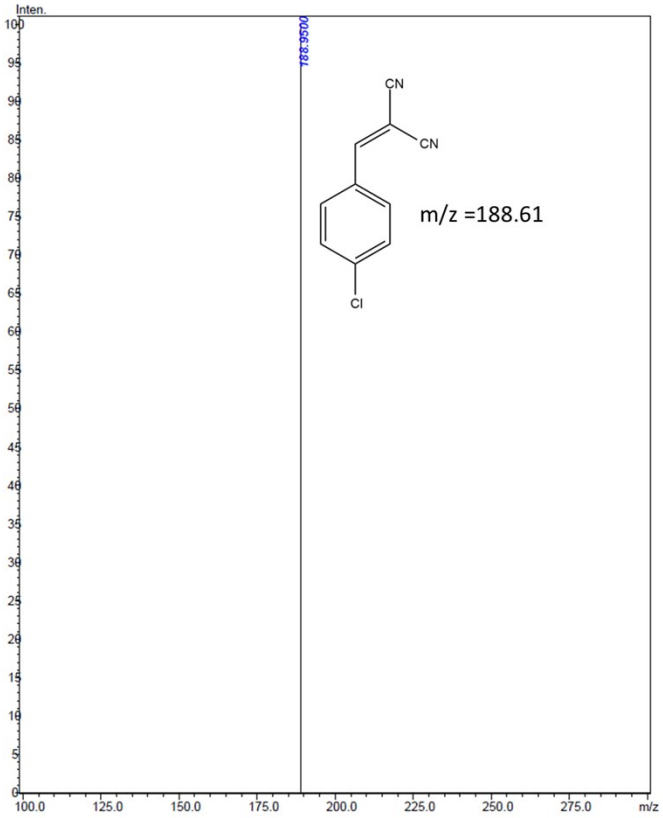

LC-MS of compound **4b**

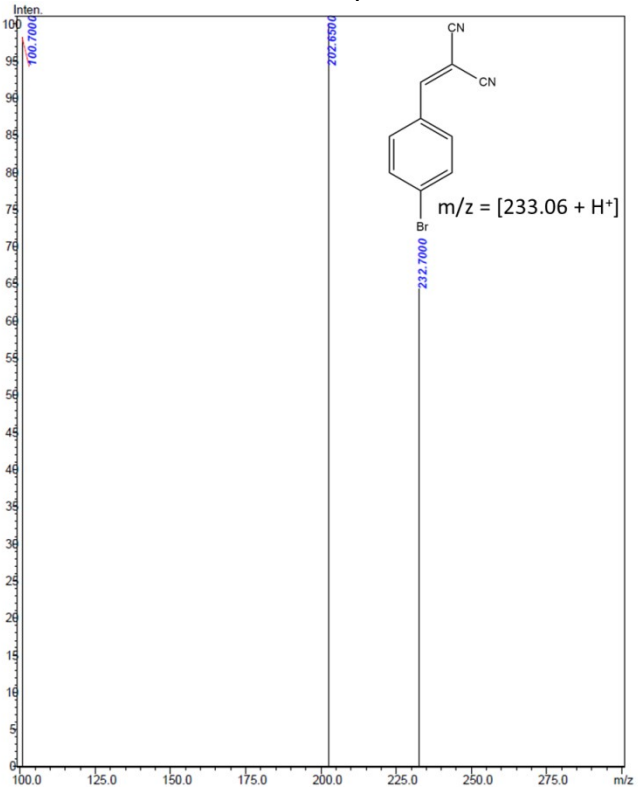

LC-MS of compound **4c**

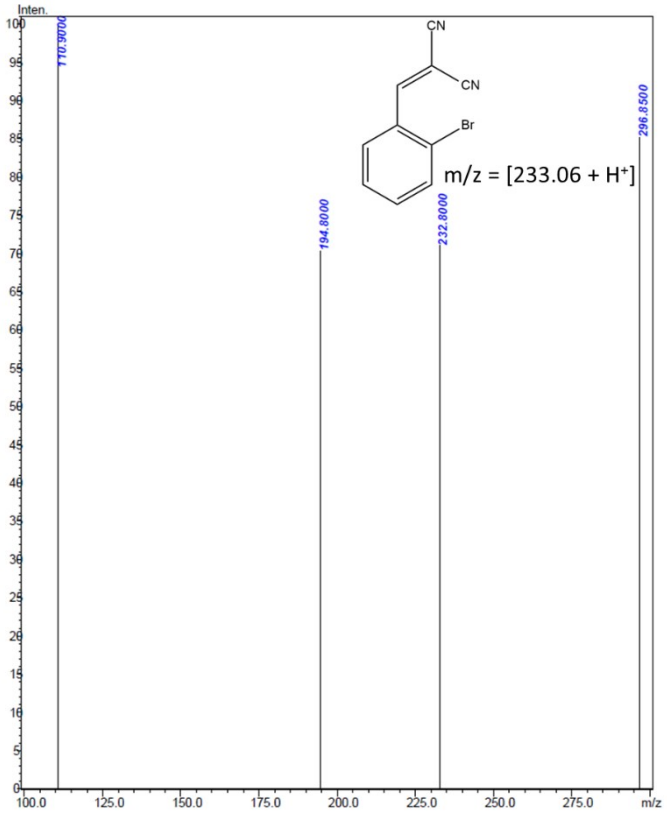

LC-MS of compound **4d**

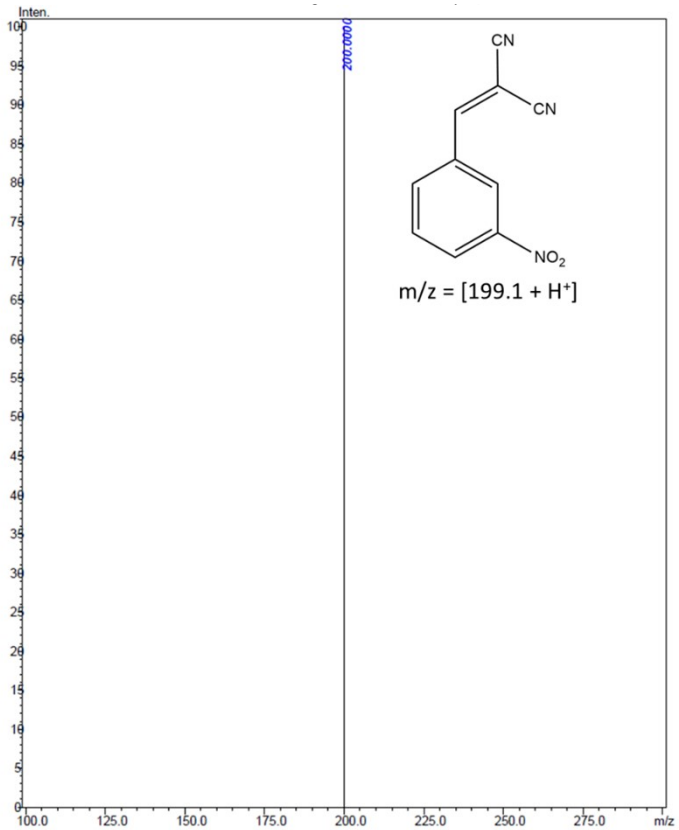

LC-MS of compound **4e**

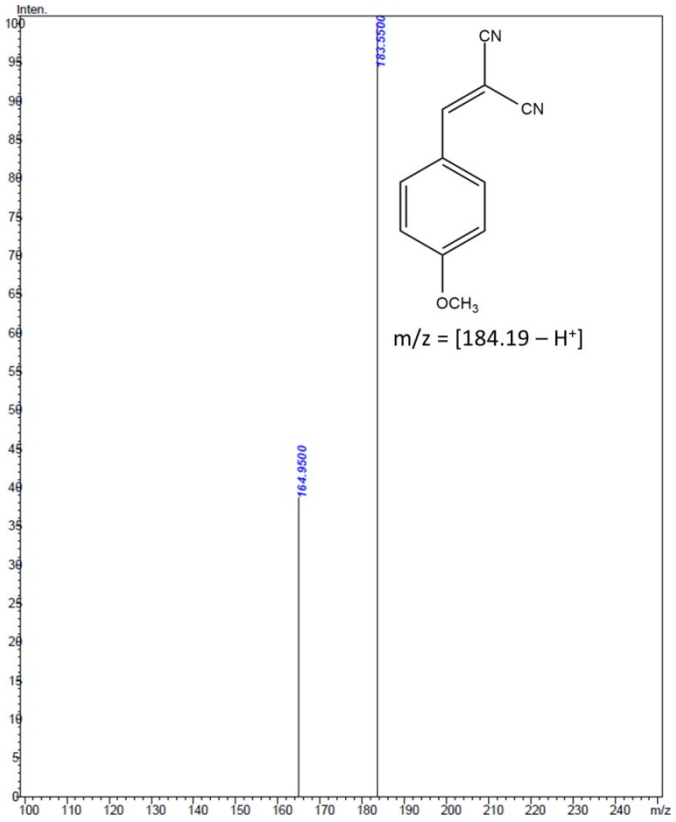

LC-MS of compound **4f**

Table S6. Deacetalization/Knoevenagel condensations reaction catalysed by various bifunctional catalysts

Catalyst	Active sites	Solvent	Reaction Condition	Yield (%)	Ref
MIL-101(Cr)@CS nanoparticles	Amino and hydroxyl groups	Acetonitrile/H_2O	Temp: 80°C Time: 12 h.	99	11
PCN-222-Co@TpPa-1.	Co(II), Zr(IV) and Imine group	DMSO-d_6	Temp: 50°C Time: 10 h.	99.3	12
IRA900(0.2OH)-MIL-101(Al)−NH_2	Al(III) and NH_2	Toluene	Temp: 110°C Time: 5 h.	99	13
MIL-101(Al/Fe)-NH_2	Al/Fe and NH_2	Toluene	Temp: 120°C Time: 12 h	99.9	14
Fe_3O_4/PVP–PWA(141)	Fe_3O_4	Acetic acid/H_2O	Temp: 80°C Time: 4 h	98	15
ZIF8-A61-SO_3H	NH_2 and SO_3H	1,4-dioxane/H_2O	Temp: 80°C Time: 4 h	98	16
MIL-101-AB-x	NH_2 and SO_3H	DMF	Temp: 90°C Time: 2 h	98	17
UiO-66@SNW-1	Zr/Aminal groups	DMSO-d_6	Temp: 80°C Time: 12 h	99.6	18
SO_3H-AA@MNP	NH_2 and SO_3H	Toluene	Temp: 90°C Time: 10 h	99	19
P(DVB–NH_2–n-StSO_3H)	NH_2 and SO_3H	Toluene/H_2O	Temp: 80°C Time: 24 h	99	20
HMSAl@MS-NH_2	Al(III) and NH_2	Toluene	Temp: 110°C Time: 20 min	100	21
Yb-BDC-NH_2	Yb/NH_2	DMSO-d_6	Temp: 50°C Time: 24 h	97	22
Al-POSS-NH_2	Al(III) and NH_2	DMF	Temp: 80°C Time: 6 h	99	This work

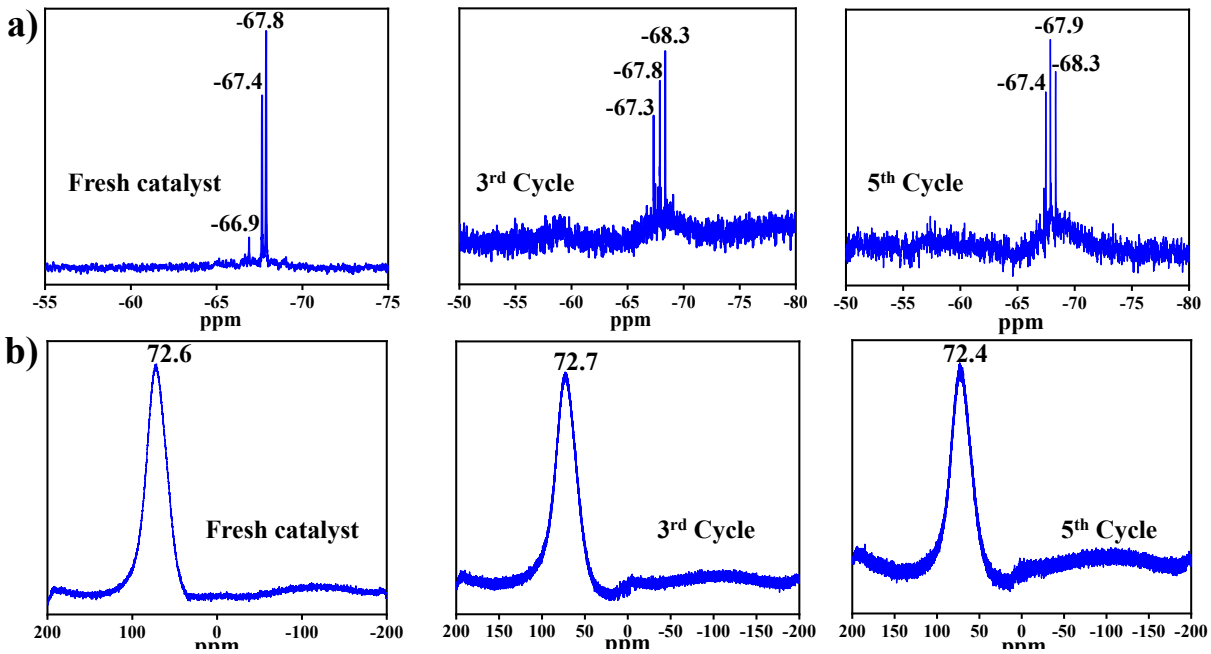

Fig. S8 (a) ^{29}Si NMR and (b) ^{27}Al NMR spectra of freshly prepared catalyst, reused catalyst after third and fifth cycles.

Table S7. Optimization of deketalization -Knoevenagel condensation reaction

Entry	Solvent	Catalyst (mol%)	Time (hours)	Isolated Yield (%)	TON
1	DMF	3	8	25	83
			16	38	126
			24	40	133
2	DMF	6	8	36	60
			16	88	146
			24	88	146

One-pot Tandem Deketalization-Knoevenagel Condensation Reactions

^{1}H NMR Spectra:

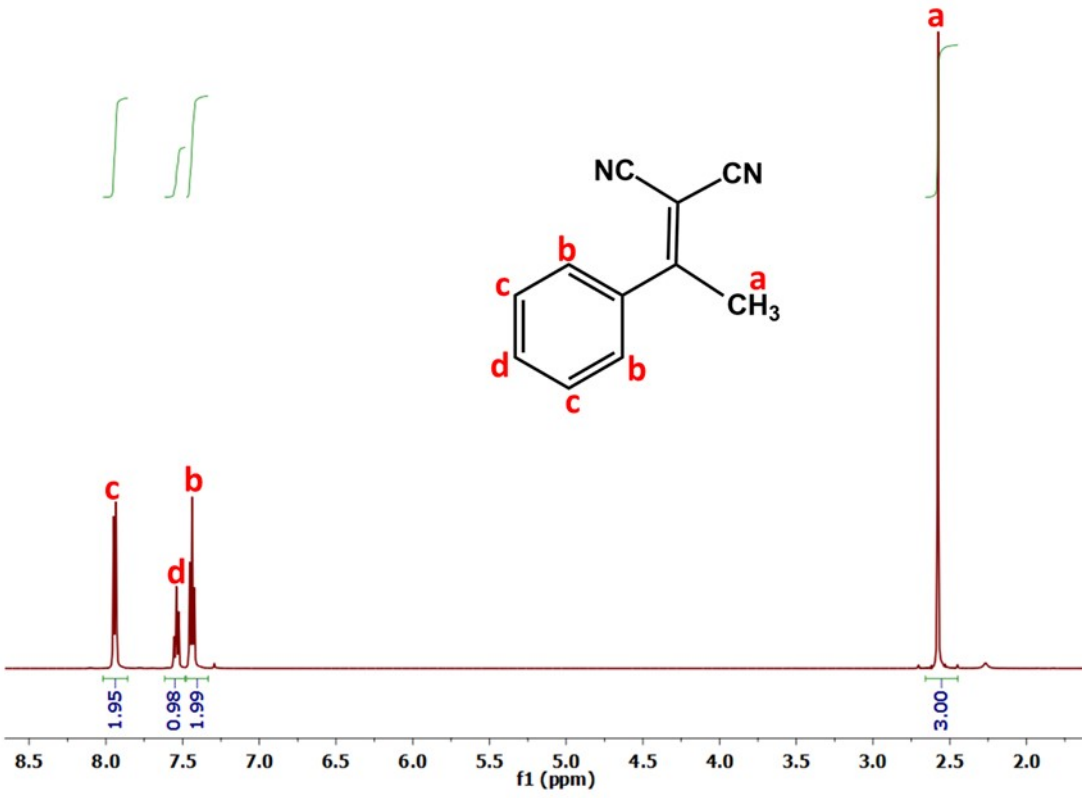

^{1}H NMR spectrum of compound **6** in $CDCl_3$

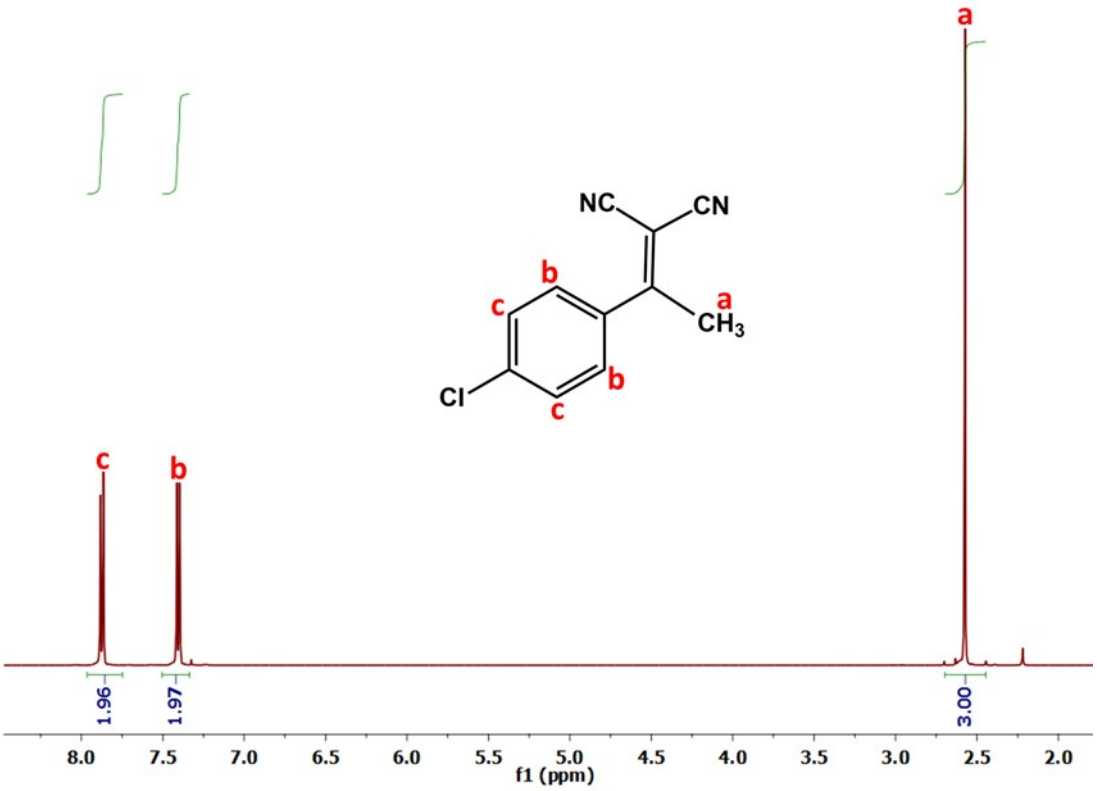

^{1}H NMR spectrum of compound **6a** in $CDCl_3$

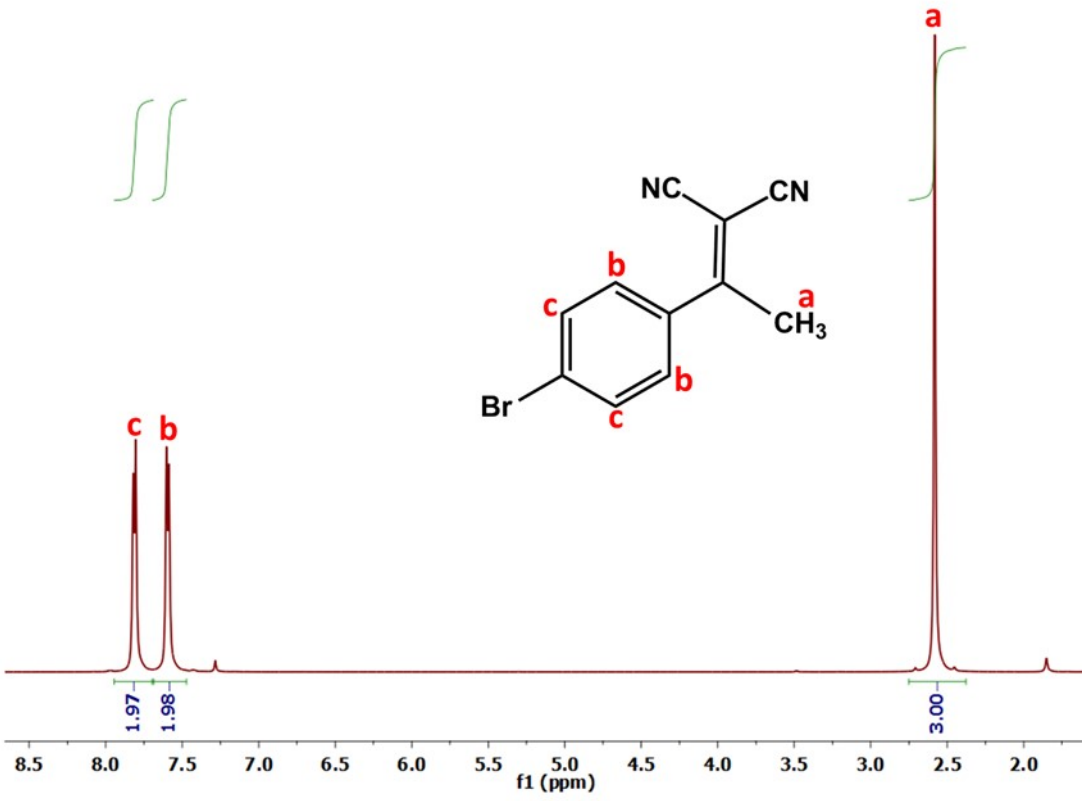

^{1}H NMR spectrum of compound **6b** in $CDCl_3$

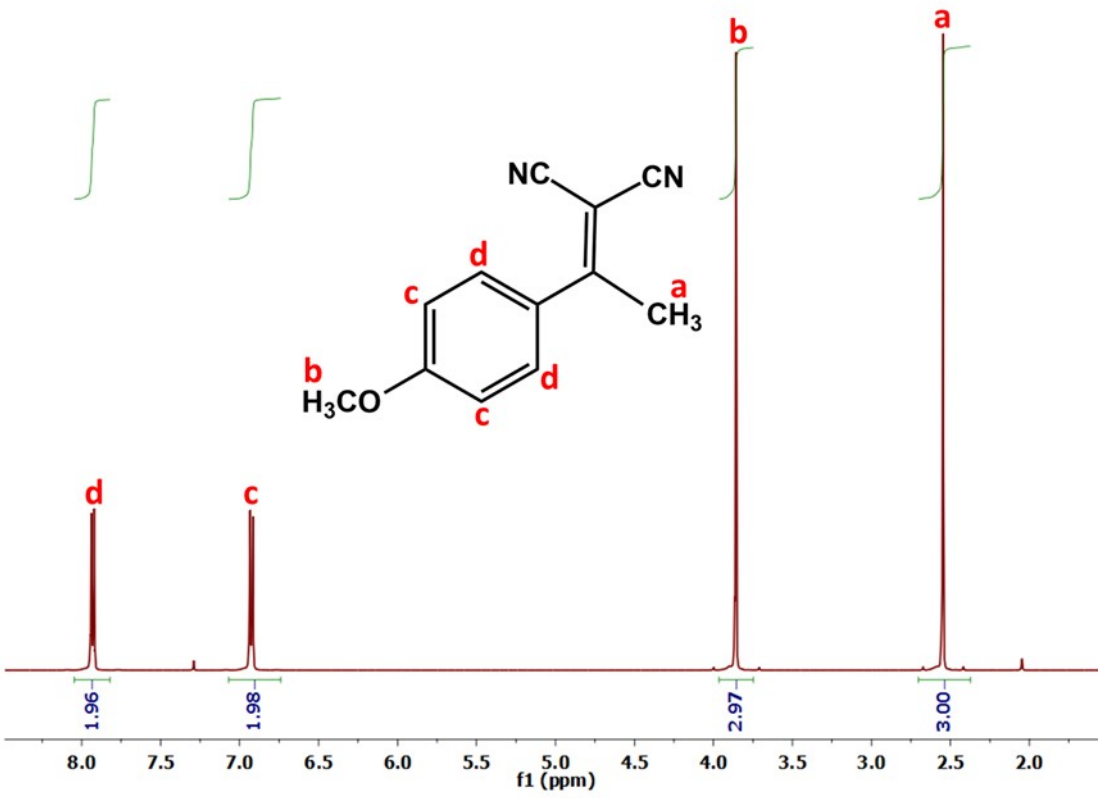

^{1}H NMR spectrum of compound **6c** in $CDCl_3$

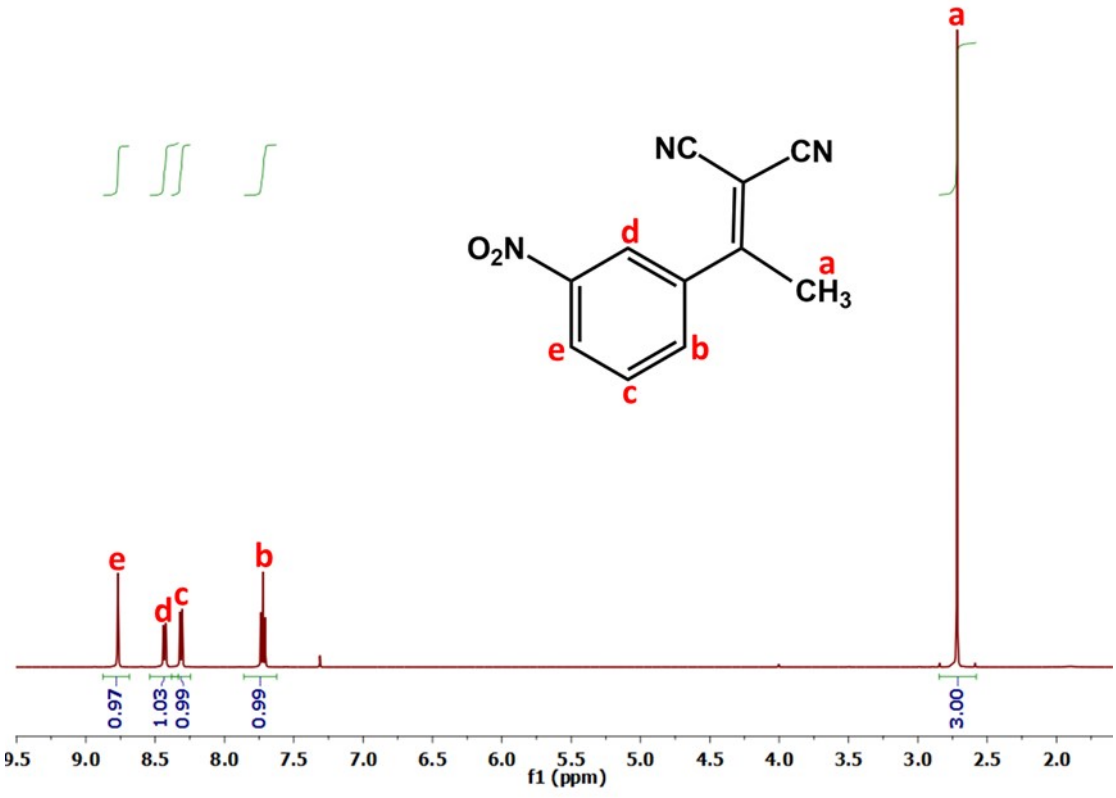

^{1}H NMR spectrum of compound **6d** in $CDCl_3$

^{13}C NMR Spectra:

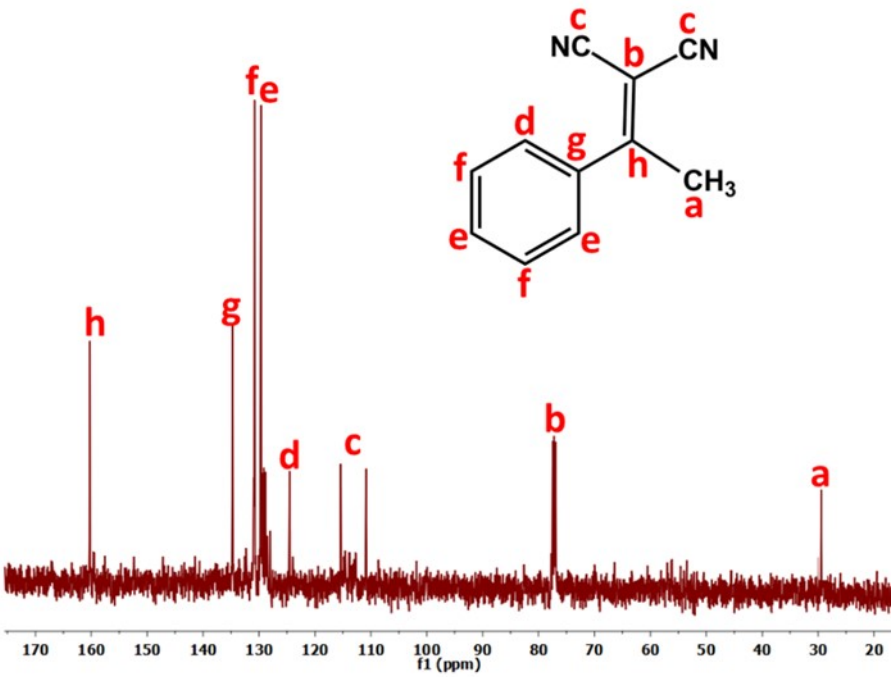

^{13}C NMR spectrum of compound **6** in $CDCl_3$

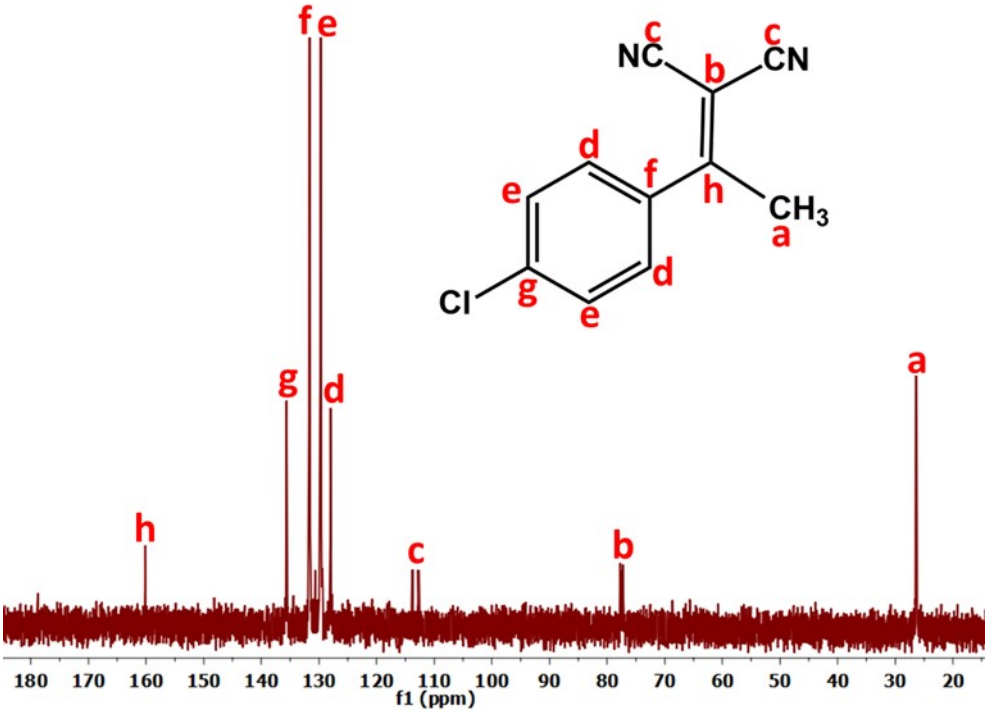

^{13}C NMR spectrum of compound **6a** in $CDCl_3$

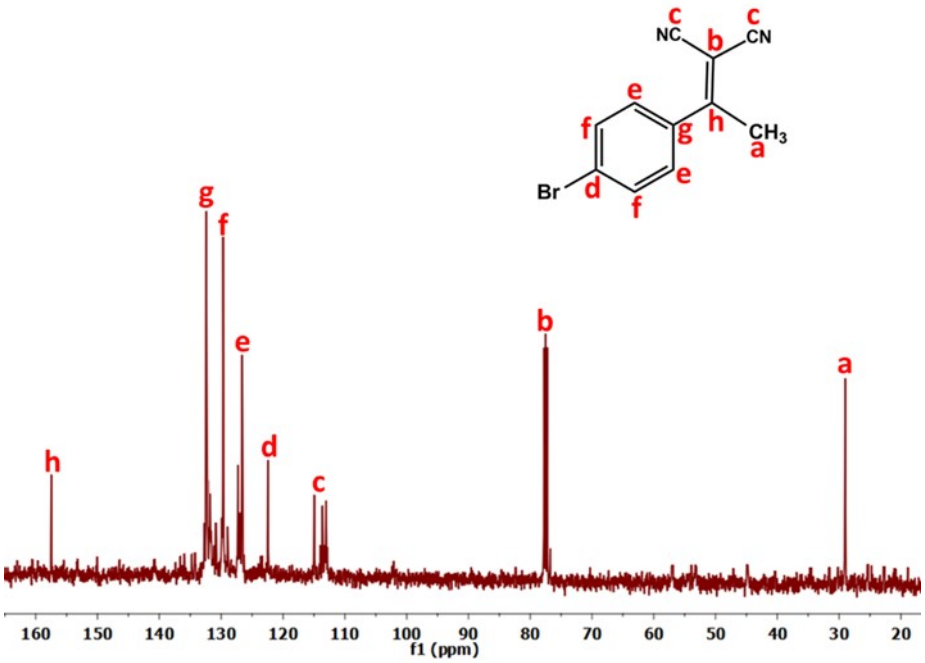

^{13}C NMR spectrum of compound **6b** in $CDCl_3$

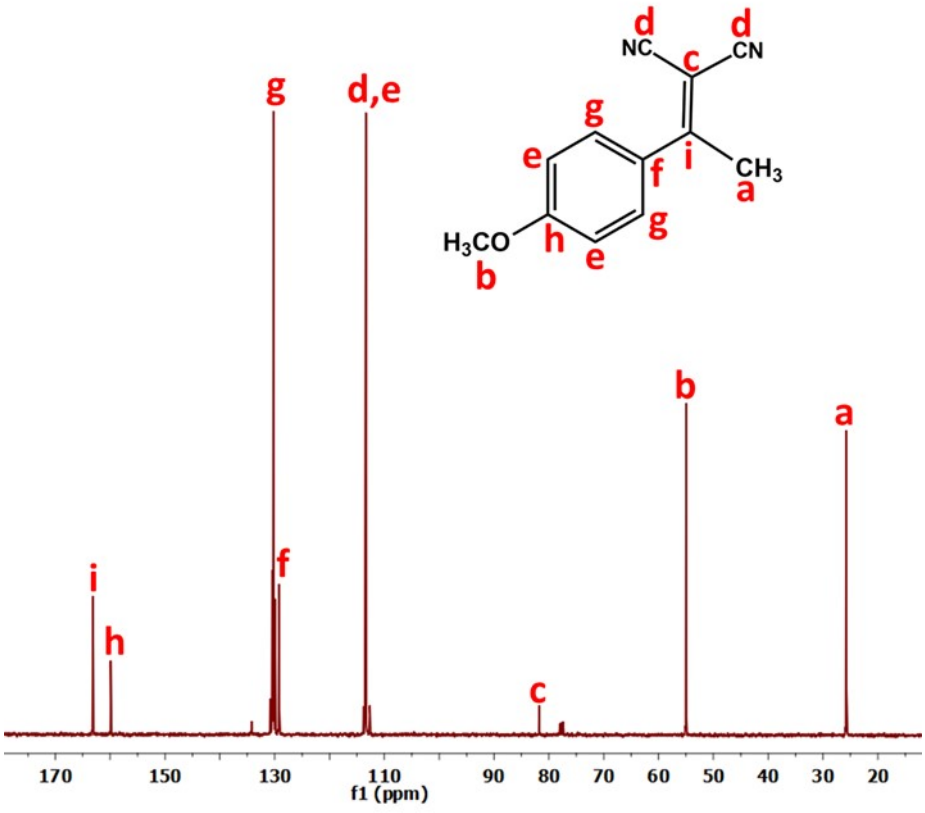

^{13}C NMR spectrum of compound **6c** in $CDCl_3$

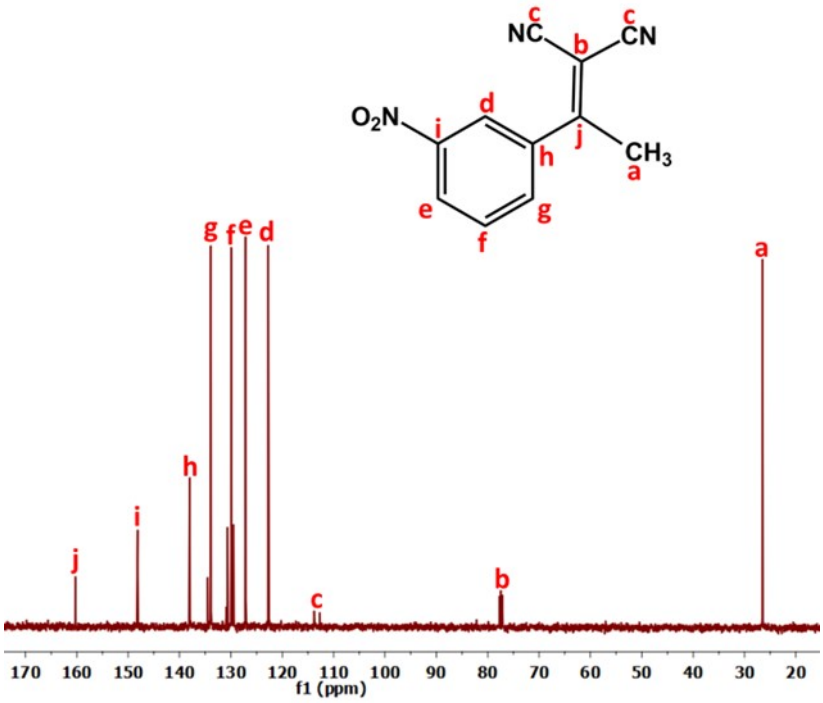

^{13}C NMR spectrum of compound **6d** in $CDCl_3$

LC-MS:

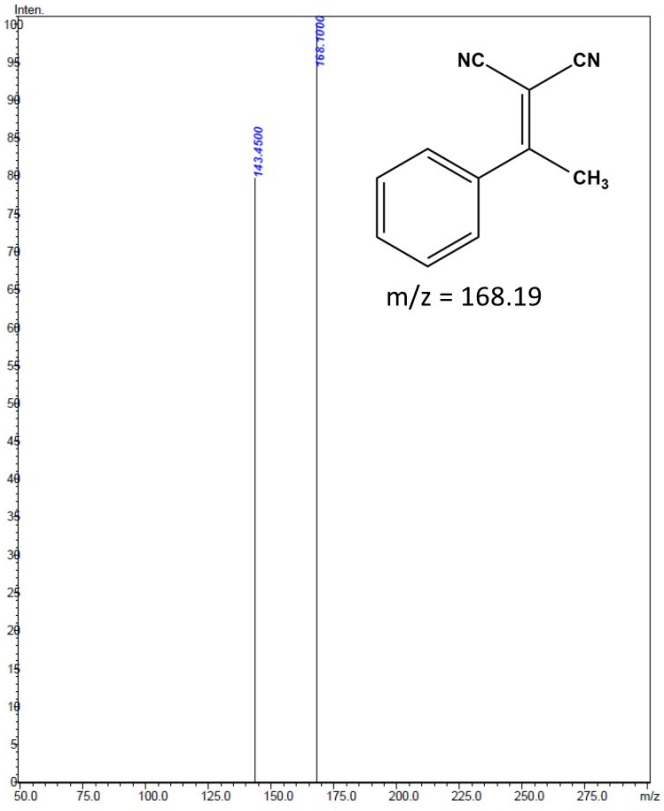

LC-MS of compound **6**

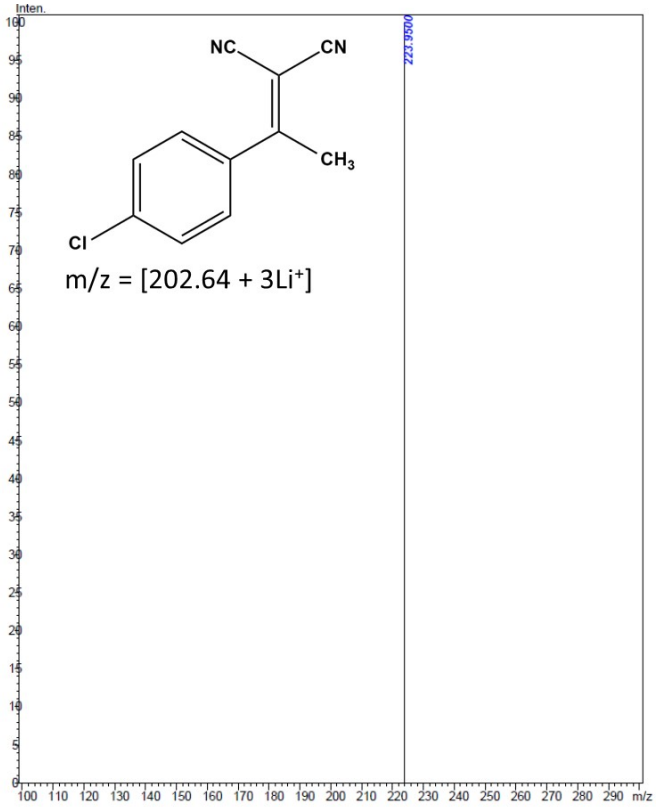

LC-MS of compound **6a**

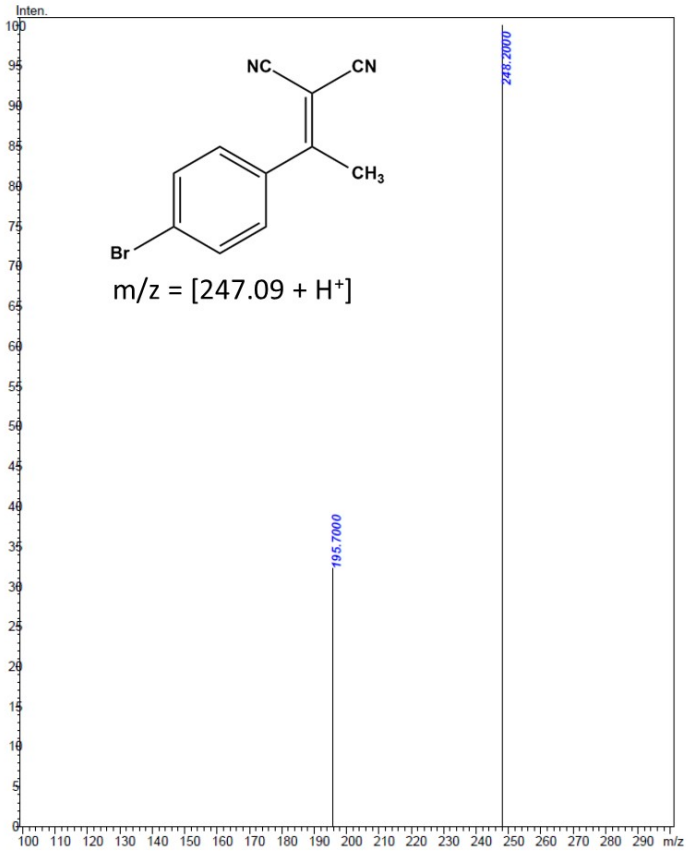

LC-MS of compound **6b**

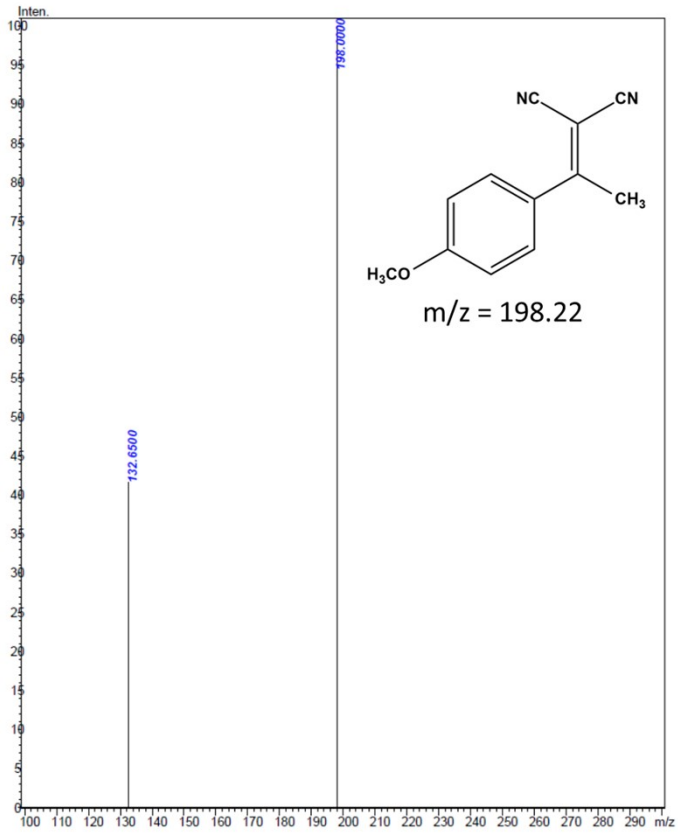

LC-MS of compound **6c**

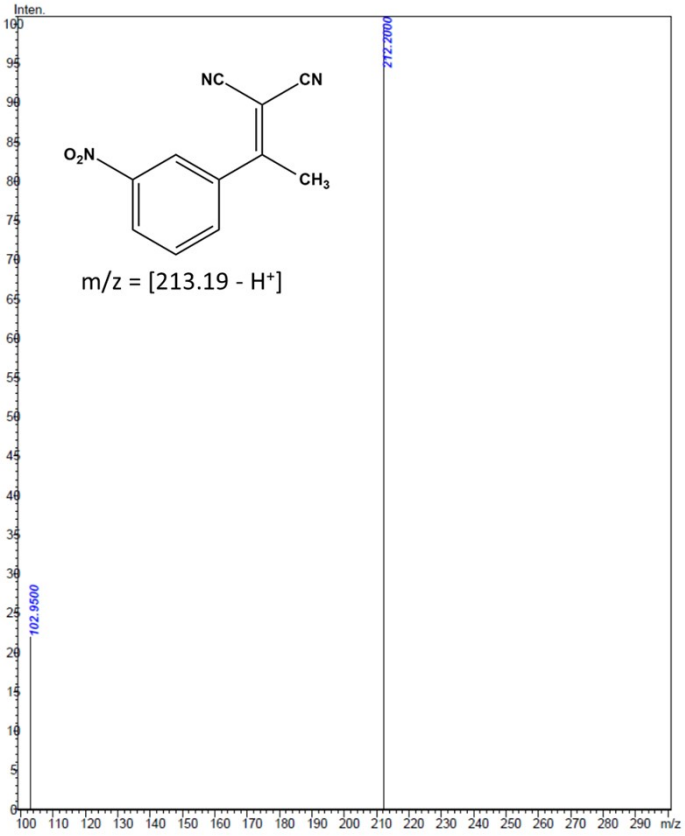

LC-MS of compound **6d**

^{1}H, ^{13}C NMR and LC-MS of 2-(4-hydroxy-3-methoxybenzylidene)malononitrile

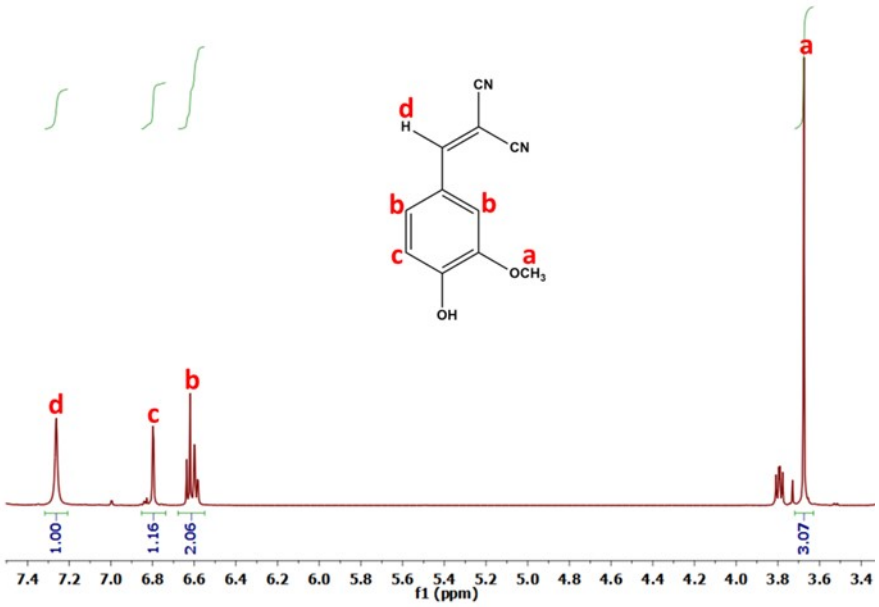

^{1}H NMR spectrum of 2-(4-hydroxy-3-methoxybenzylidene)malononitrile in DMSO-d6

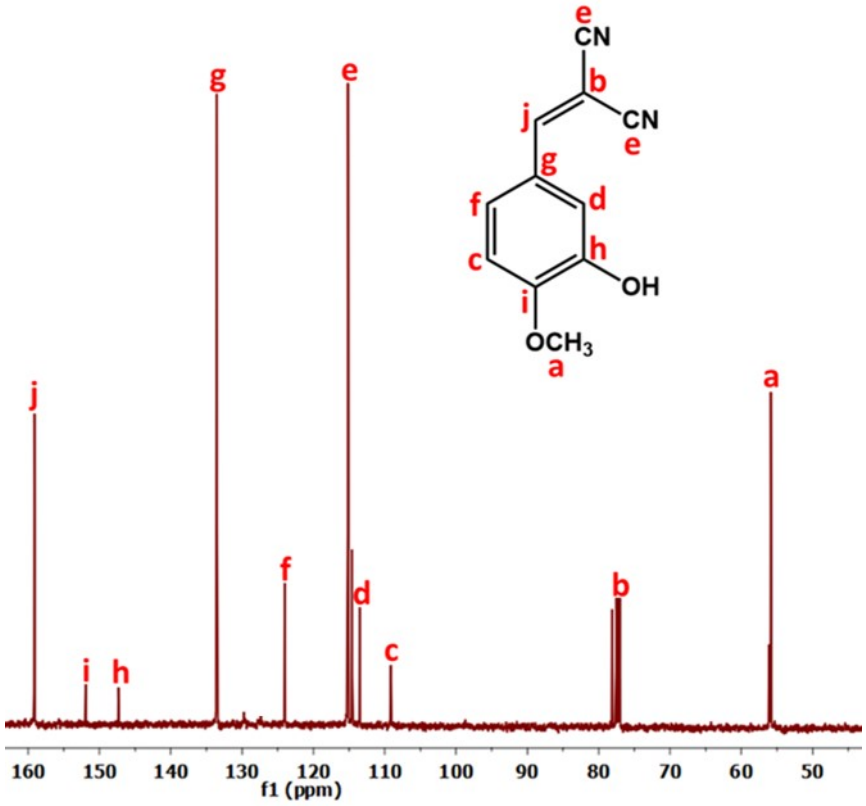

^{13}C NMR spectrum of 2-(4-hydroxy-3-methoxybenzylidene)malononitrile in DMSO-d6

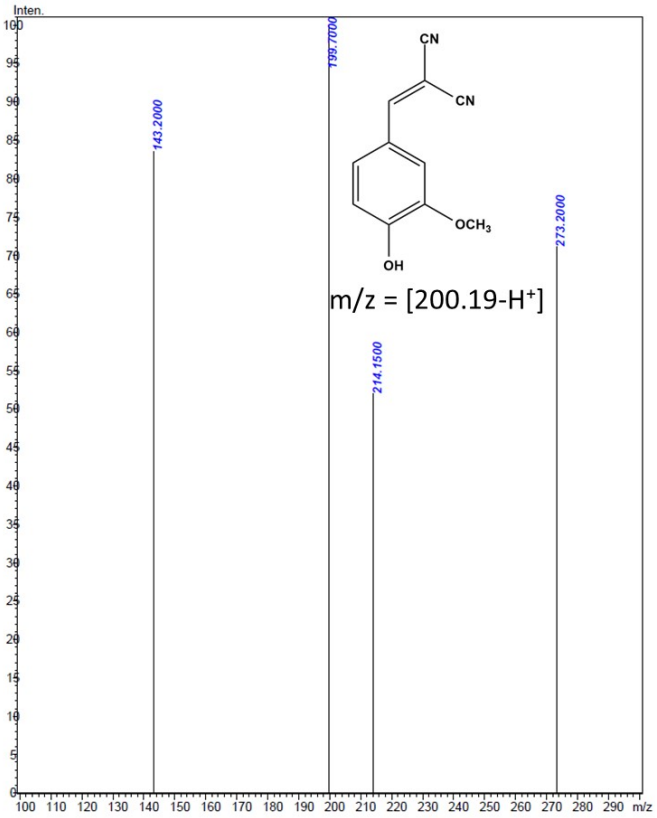

LC-MS of 2-(4-hydroxy-3-methoxybenzylidene)malononitrile

Synthesis of 2-aryl-2-methyl-1,3-dioxolane (cyclic ketals) (5–5d)

The cyclic ketals were synthesized based on previously reported procedure with slight modification.[23] Acetophenone or substituted acetophenone (0.01 mol), ethylene glycol (3.1 g, 2.8 ml, 0.05 mol), and *p*-toluene sulfonic acid (0.052 g, 0.0003 mol) in benzene (40 ml) were added to a dry 100 ml double neck round bottom flask equipped with the Dean-Stark apparatus. The reaction mixture was reflux for 48 hours for the removal of azeotropic water and the solvent was removed under reduced pressure. Then, the crude product was further was further dissolved with ether and washed with aqueous $NaHCO_3$ solution. The organic layer was separated and dried over $MgSO_4$ for overnight, and filtered. The filtrate was evaporated under reduced pressure to obtain a pale-yellow solid of products. Subsequently, the resultant pale-yellow solid was further purified by column chromatography using hexane as an eluent. The resultant cyclic ketals were confirmed by ^1H NMR and LC-MS.

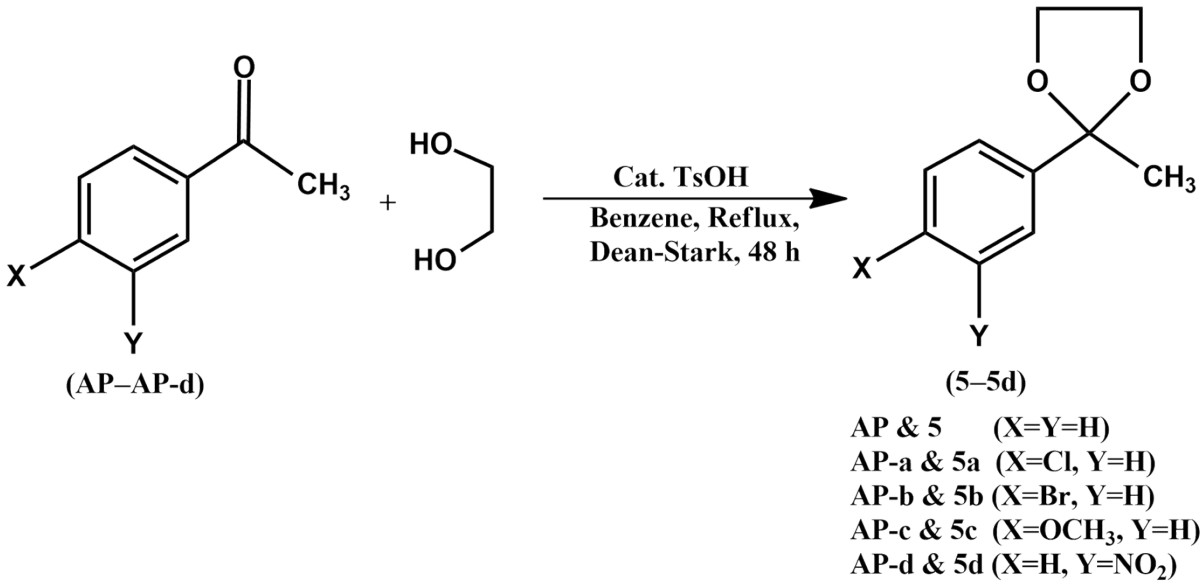

(AP–AP-d)

(5–5d)

AP & 5 (X=Y=H)
AP-a & 5a (X=Cl, Y=H)
AP-b & 5b (X=Br, Y=H)
AP-c & 5c (X=OCH_3, Y=H)
AP-d & 5d (X=H, Y=NO_2)

Scheme S1. Synthesis of cyclic ketals (**5–5d**).

^{1}H NMR Spectra

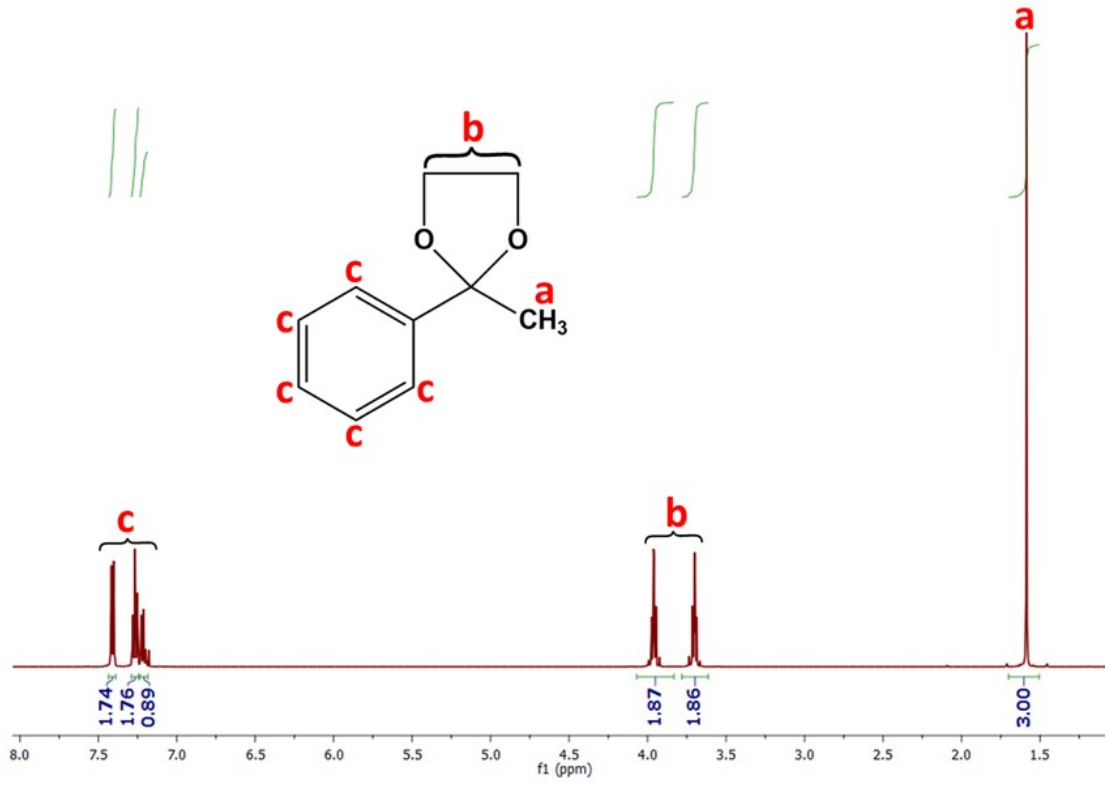

^{1}H NMR spectrum of compound **5** in $CDCl_3$

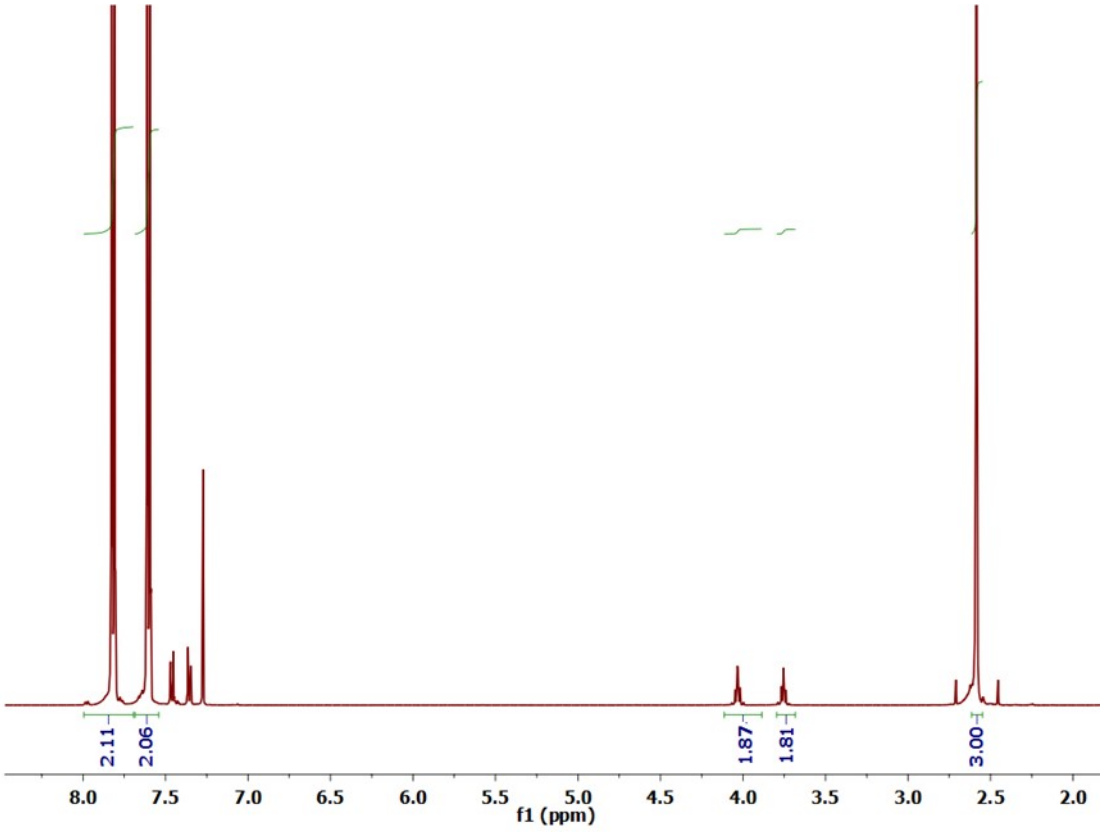

^{1}H NMR spectrum of compound **5a** in $CDCl_3$

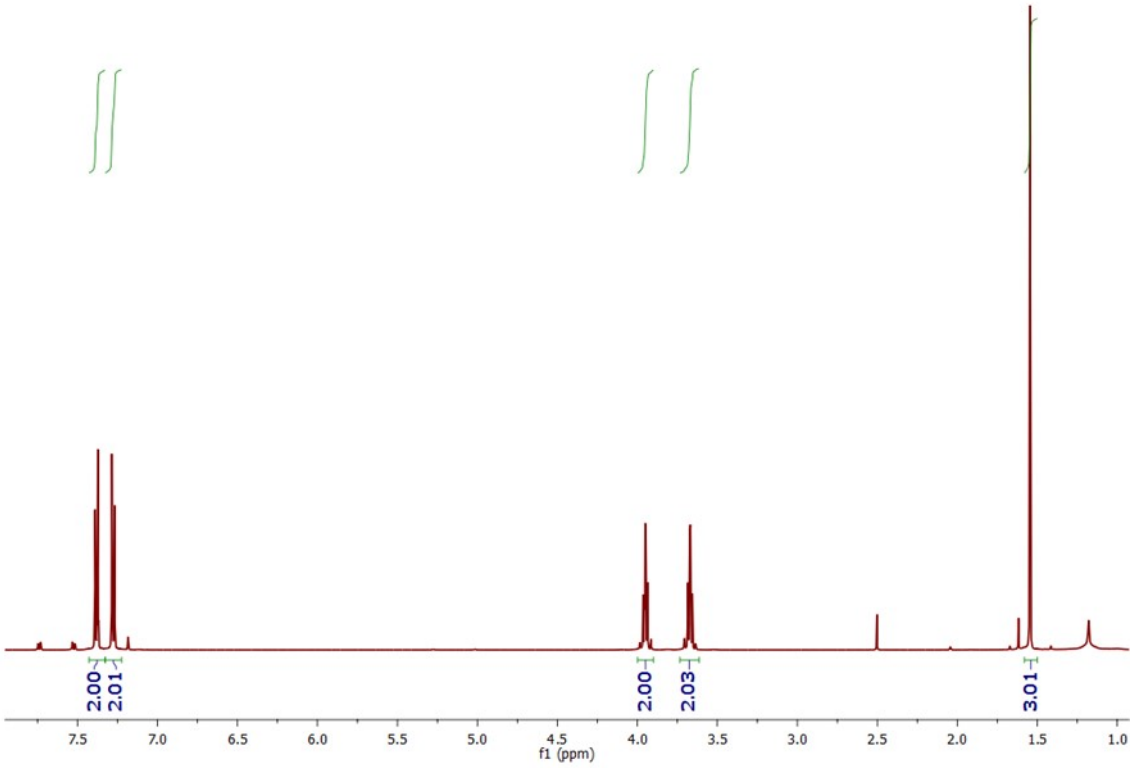

^{1}H NMR spectrum of compound **5b** in $CDCl_3$

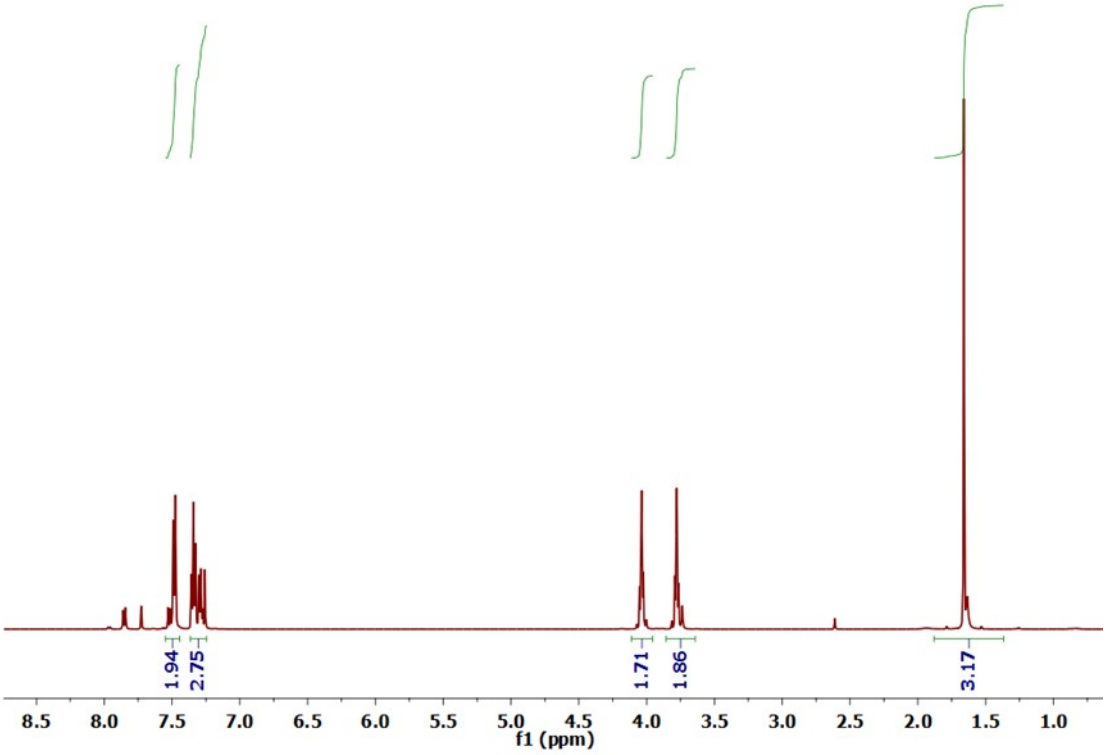

^{1}H NMR spectrum f compound **5c** in $CDCl_3$

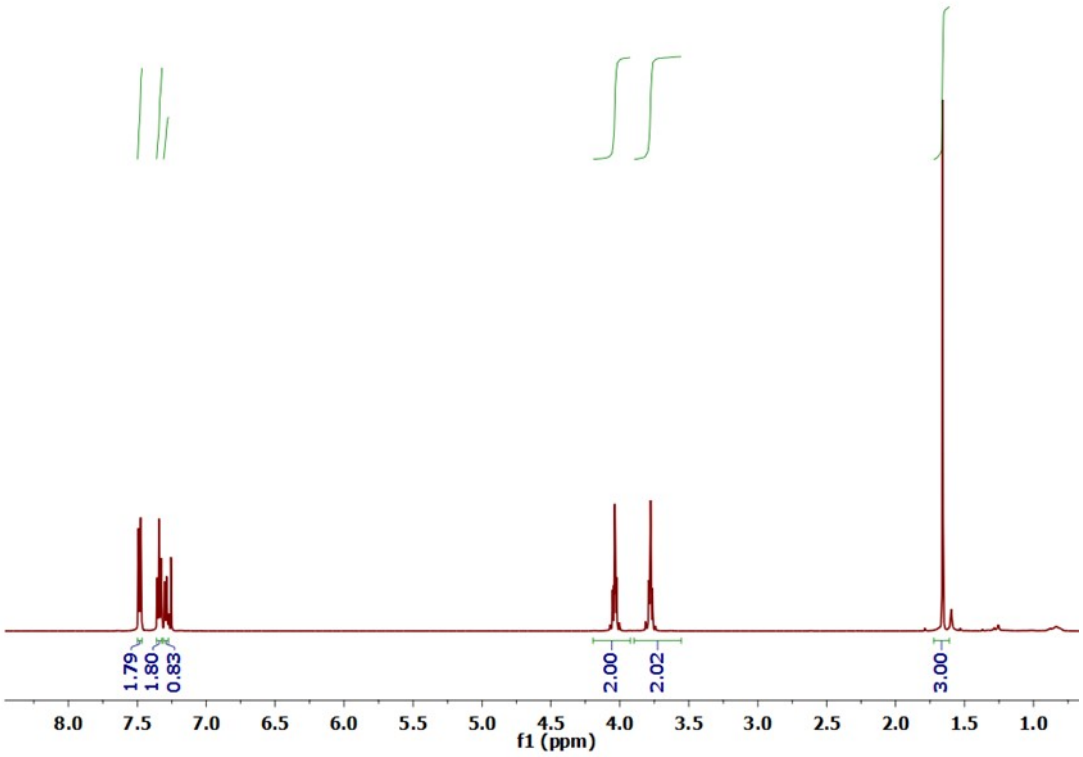

^{1}H NMR spectrum of compound **5d** in $CDCl_3$

LC-MS:

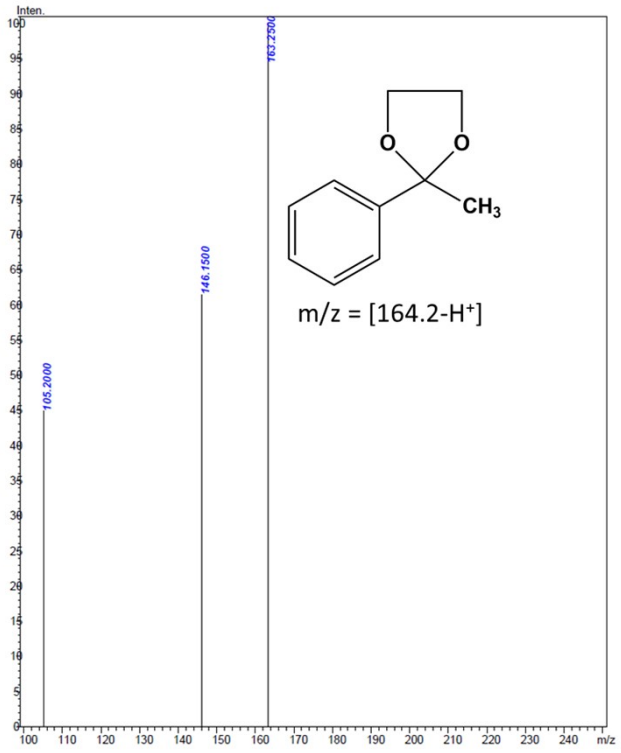

LC-MS of compound **5**

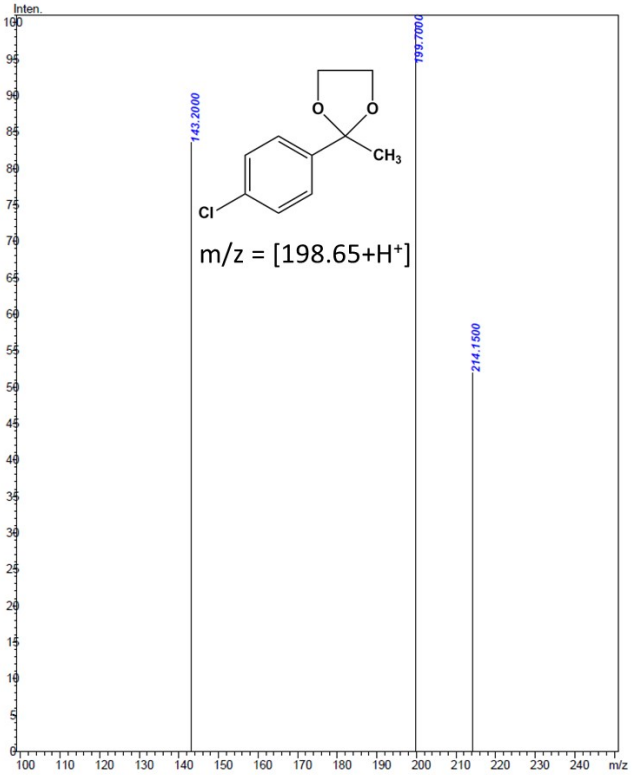

LC-MS of compound **5a**

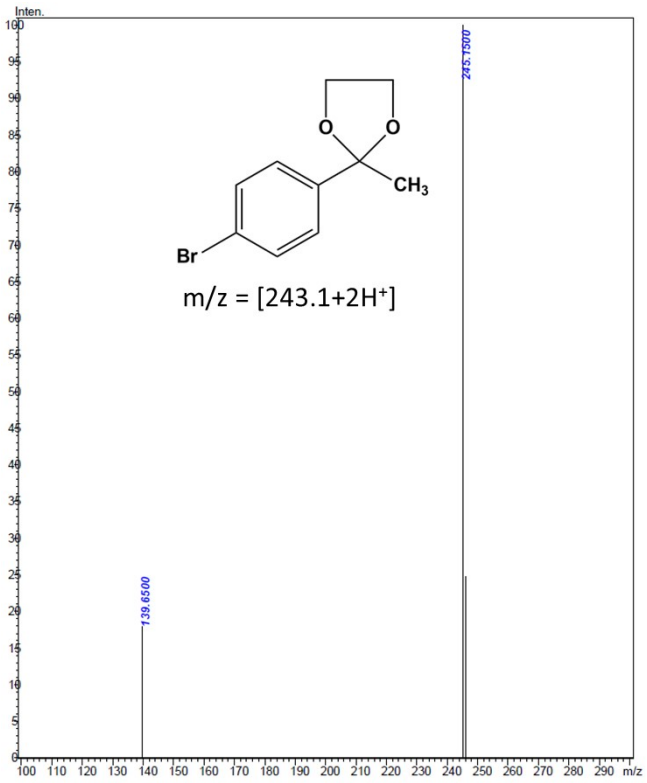

LC-MS of compound **5b**

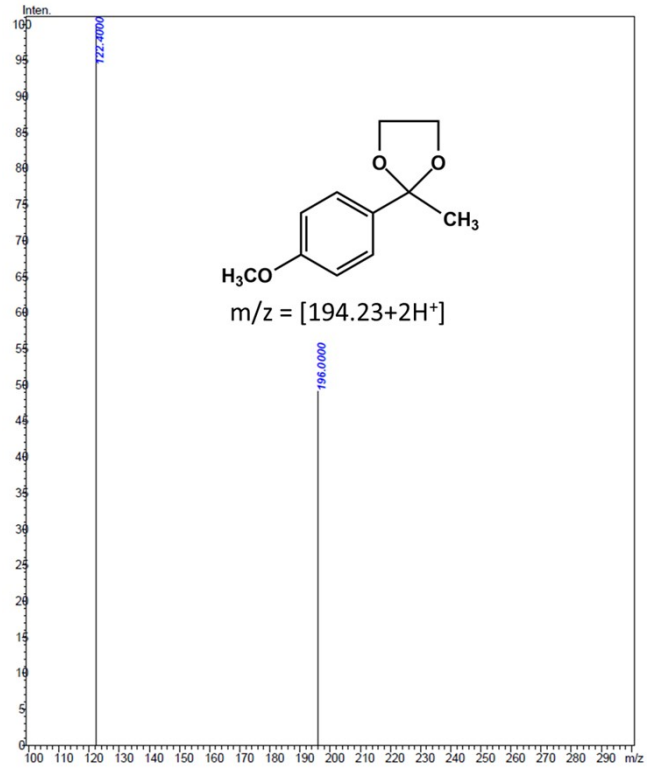

LC-MS of compound **5c**

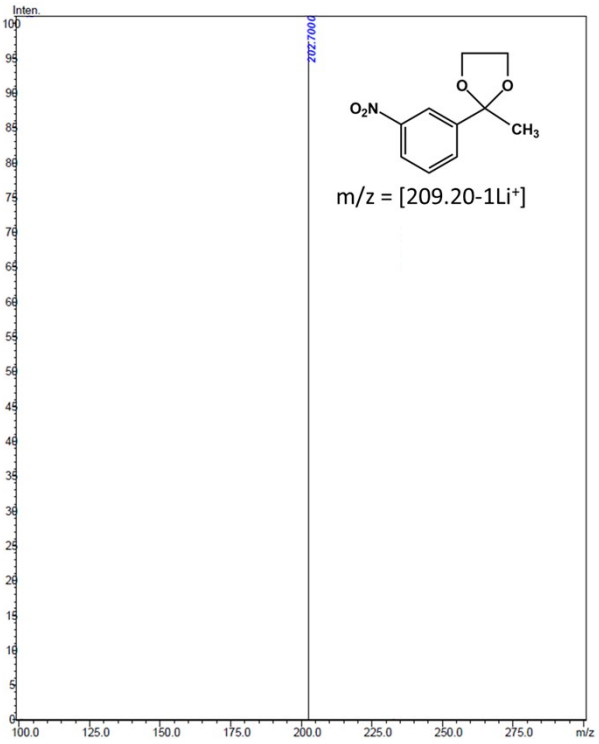

LC-MS of compound **5d**

Synthesis of vanillin acetal

The vanillin acetal was synthesized based on previously reported procedure with slight modification.[23] 4-hydroxy-3-methoxybenzaldehyde (2.4 g, 0.015 mol), ethylene glycol (3.1 g, 2.8 ml, 0.05 mol), and *p*-toluene sulfonic acid (0.065 g, 0.0004 mol) in benzene (40 ml) were added to a dry 100 ml double neck round bottom flask equipped with the Dean-Stark apparatus. The reaction mixture was reflux for 48 hours for the removal of azeotropic water and the solvent was removed under reduced pressure. Then, the crude product was further was further dissolved with ether and washed with aqueous $NaHCO_3$ solution. The organic layer was separated and dried over $MgSO_4$ for overnight, and filtered. The filtrate was evaporated under reduced pressure to obtain a pale yellow solid of product. Subsequently, the resultant pale yellow solid was further purified by column chromatography using hexane as an eluent. Yield: 41 %. The resultant cyclic acetal was confirmed by ^1H NMR and LC-MS.

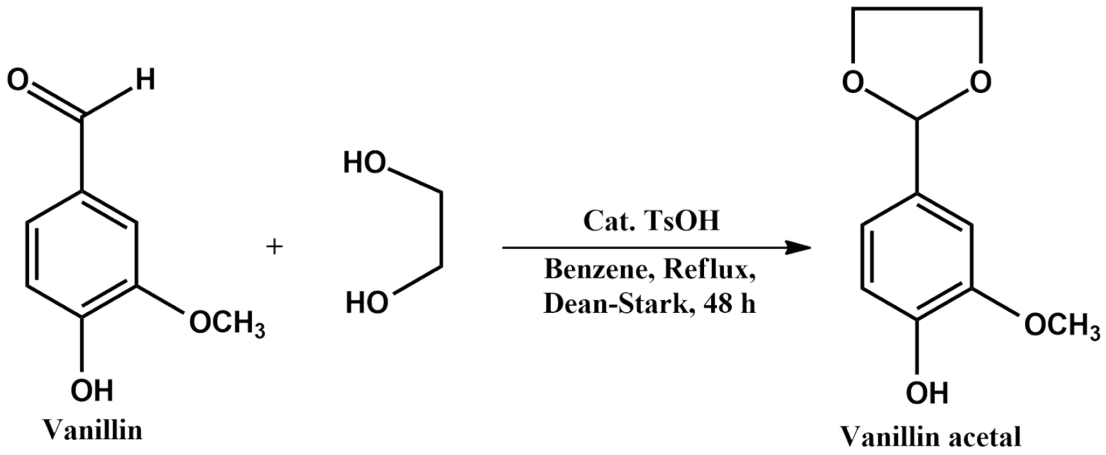

Scheme S2. Synthesis of vanillin acetal

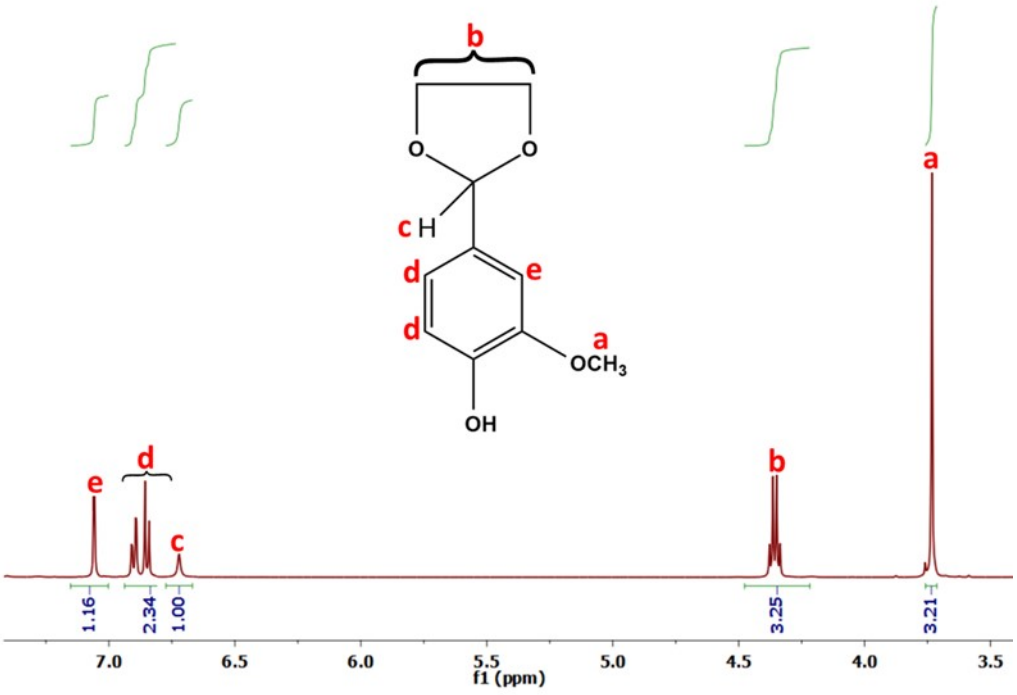

^{1}H NMR spectrum of vanillin acetyl in DMSO-d6.

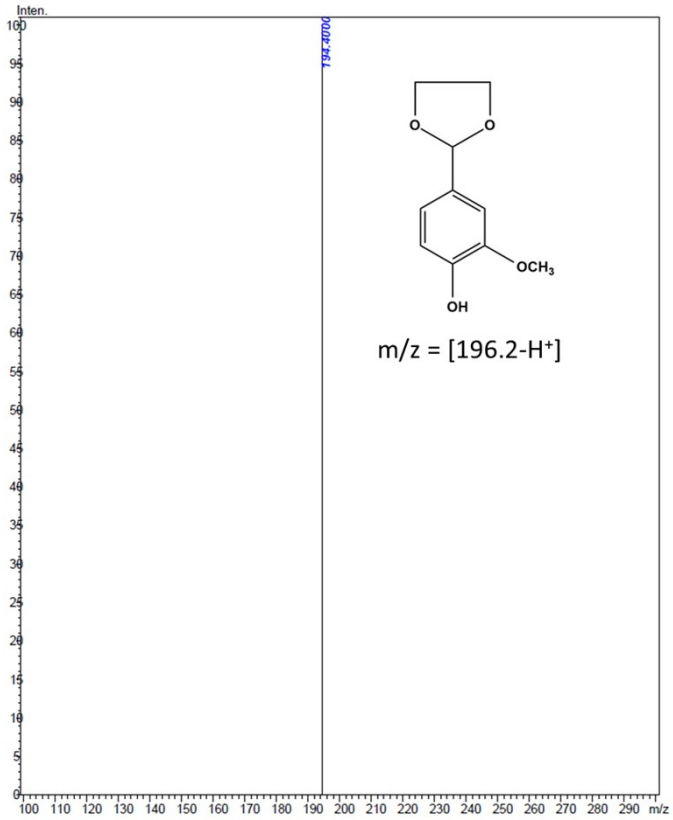

LC-MS of vanillin acetal

References

1. J. VandeVondele, M. Krack, F. Mohamed, M. Parrinello, T. Chassaing and J. Hutter, Quickstep: fast and accurate density functional calculations using a mixed gaussian and plane waves approach, *Comput. Phys. Commun*., 2005, **167***,* 103–128.
2. J. P. Perdew, K. Burke and M. Ernzerhof, Generalized gradient approximation made simple, *Phys. Rev. Lett*., 1996, **77***,* 3865–3868.
3. S. Grimme, Semiempirical GGA-type density functional constructed with a long-range dispersion correction, *J. Comput. Chem.,* 2006, **27***,* 1787–1799.
4. S, Grimme, Accurate description of vander waals complexes by density functional theory including empirical corrections, *J. Comput. Chem*., 2004, **25***,* 1463–1473.
5. J. VandeVondele and J. Hutter, Gaussian basis sets for accurate calculations on molecular systems in gas and condensed phases. *J. Chem. Phys.* 2007, **127***,* 114105.

6. E. J. Baerends, T. Ziegler, A. J. Atkins, J. Autschbach, O. Baseggio, D. Bashford, A. Bérces, F. M. Bickelhaupt, C. Bo, P. M. Boerrigter, C. Cappelli, L. Cavallo, C. Daul, D. P. Chong, D. V. Chulhai, L. Deng, R. M. Dickson, J. M. Dieterich, F. Egidi and D. E. Ellis, AMS. A. L. Y. ADF 2019, **305**, SCM.
7. E. van Lenthe, E. J. Baerends and J. G. Snijders, Relativistic total energy using regular approximations. *J. Chem. Phys.,* 1994, **101***,* 9783–9792.
8. R. F. W. Bader, Atoms in molecules, *Acc. Chem. Res.,* 1985, **18***,* 9–15.
9. R. F. W. Bader, A. Quantum theory of molecular structure and its applications. *Chem. Rev.* 1991, **91***,* 893–928.
10. C. Fonseca Guerra, J.-W. Handgraaf, E. J, Baerends and F. M. Bickelhaupt, Voronoi deformation density (VDD) charges: assessment of the mulliken, bader, hirshfeld, weinhold, and VDD methods for charge analysis, *J. Comput. Chem.,* 2004, **25***,* 189–210.
11. Z. S. Zhao, Y. Zhang, T. Fang, Z. B. Han and F. S. Liang, Chitosan-Coated Metal-Organic-Framework Nanoparticles as Catalysts for Tandem Deacetalization-Knoevenagel Condensation Reactions, *ACS Appl. Nano Mater.,* 2020, **3**, 6316–6320.
12. M.-L. Gao, M.-H. Qi, L. Liu and Z.-B. Han, An exceptionally stable core–shell MOF/COF bifunctional catalyst for a highly efficient cascade deacetalization–Knoevenagel condensation reaction, *Chem. Commun.,* 2019, **55**, 6377-6380.
13. Y. Hu, J. Zhang, Z. Wang, H. Huo, Y. Jiang, X. Xu, and K. Lin, Ion-Exchange Fabrication of Hierarchical Al-MOF-Based Resin Catalysts for the Tandem Reaction, *ACS Appl. Mater. Interfaces,* 2020, **12**, 36159−36167.
14. Y. Hu, J. Zhang, H. Huo, Z. Wang, X. Xu, Y. Yang, K. Lin and R. Fan, One-pot Synthesis of Bimetallic Metal-Organic Frameworks (MOFs) as Acid-Base Bifunctional Catalysts for Tandem Reaction*, Catal. Sci. Technol.,* 2020, **10**, 315–322.

15. S. B. Kamble, and C. V. Rode, Cascade Synthesis of 2-Cyanoacrylamides through Deacetalization and/or Knoevenagel Condensation followed by Selective Monohydration of Acetals and Aldehydes over Solid Acid Ferrites, *ChemCatChem,* 2016, **8**, 2678.
16. Y.R, Lee, X.H, Do, S.S, Hwang, K.Y, Baek, Dual-functionalized ZIF-8 as an efficient acidbase bifunctional catalyst for the one-pot tandem reaction, *Catal Today*, 2019, **359**, 124–132.
17. H. Liu, F. G. Xi, W. Sun, N. N. Yang and E. Q. Gao, Amino- and sulfo-bifunctionalized metal−organic frameworks: one- pot tandem catalysis and the catalytic sites, *Inorg. Chem.,* 2016, **55**, 5753–5755.
18. M. Qi, M. Gao, L. Liu and Z. Han, Robust Bifunctional Core−Shell MOF@POP Catalyst for One-Pot Tandem Reaction, *Inorg. Chem.,* 2018, **57**, 14467–14470.
19. 3 Z. Wang, X. Yuan, T. Zhang and J. Luo, An efficient and recyclable acid–base bifunctional core–shell nano-catalyst for the one-pot deacetalization–Knoevenagel tandem reaction, *New J. Chem.,* 2018, **42**, 11610–11615.
20. Z. Sun, X. Yang, X. Huang, M. Zhang, G. Bian, Y. Qi, X. Yang and W. Zhang, Mesoporous polymeric catalysts with both sulfonic acid and basic amine groups for the one-pot deacetalization-Knoevenagel reaction *New J. Chem*., 2019, **43**, 16676−16684.
21. C. You, C. Yu, X. Yang, Y. Li, H. Huo, Z. Wang, Y. Jiang, X. Xu and K. Lin, Double-shelled hollow mesoporous silica nanosphere as acid-base bifunctional catalyst for cascade reactions, *New J. Chem.,* 2018, **42**, 4095–4101.
22. Y. Zhang, Y. Wang, L. Liu, N. Wei, M. L. Gao, D. Zhao and Z. B. Han, Robust Bifunctional Lanthanide Cluster Based Metal-Organic Frameworks (MOFs) for Tandem Deacetalization-Knoevenagel Reaction*, Inorg. Chem.,* 2018, **57**, 2193–2198.

23. A. R. Pinder and H. Smith, The reduction of some methyl phenyl ketones, the corresponding carbinols, and 2-methyl-2-phenyl-l: 3-dioxolans with sodium or potassium and alcohols in liquid ammonia, *J. Chem. Soc.,* 1954, 113−120.